Russian Chemical Reviews **63**(12) 977–995 (1994) ©1994 Russian Academy of Sciences and Turpion Ltd

UDC 620.193.01

Physical chemistry of the dissolution of metals

G V Khaldeev

Contents

I.	Introduction	977
II.	Dissolution and adsorption of surface-active impurities on low-angle boundaries and on grain boundaries	979
III.	Distribution of dislocations in near-surface layers of crystals	980
IV.	Current and potential oscillations during grain-boundary dissolution	983
V.	Intercrystallite corrosion	985
VI.	Dissolution of heterophase polycrystalline metals	990
VII.	Conclusion	994

Abstract. New theoretical and experimental data on the grain-boundary dissolution process in polycrystalline metals are reviewed. The original effects during transcrystallite dissolution are discussed, the basic models are analysed, and the localisation mechanism of the dissolution process on the phase bondaries of polycrystals is described. The bibliography includes 86 references.

I. Introduction

Internal boundaries in metallic crystals include low-angle boundaries formed by dislocations, grain boundaries (GB), and phase boundaries between inclusions and the matrix. In addition to the creation of strong fields due to the elastic distortion of the metal lattice (M), chemical heterogeneity is a characteristic property of these defects of the solid state. The electrochemical etching effect is observed during the dissolution of these structures.

Among nonequilibrium planar solid-state defects, the grain boundaries play a major role in the corrosion – mechanical erosion of metals. At present the metallographic evaluation of the grain composition of polycrystalline metals is based on the selective acceleration of the etching process by the grain boundaries. The role of GB is most marked during intercrystallite corrosion, and has been studied extensively.[1–4] All these workers tried to relate the differences in chemical composition of the grain-boundary region to its enhanced rate of dissolution.

From the practical point of view the effect of the grain-boundary segregation of hydrogen on the corrosion of metals is of the greatest interest, because hydrogen (the most mobile impurity in metals) can form new hydride phases on the GB and also influence their penetrability as barriers to the passage of dislocations through the boundary during plastic deformation. By using the grain boundary theory we can obtain a quantitative estimate of the contribution of GB to the corrosion, and present a physical picture of the dissolution of polycrystals. The formation of a stable fractal structure (a closed network of etched grain boundaries) strengthens the resistance of a solid to an aggressive medium. The dissolution of surface mechanical stress raisers improves the physical and mechanical properties of metallic items. The unique adsorption properties of GB allow the use of this effect in metallurgy, microelectronics, and other technological areas.

Paradoxically, the blocking of the dissolution of grain boundaries by an inhibitor (surface-active substance, impurity, etc.) has not yet attracted adequate theoretical studies, in spite of the striking advances which have been made in our understanding of the structure of the GB (see the work of Gleiter, Baluffi, Chadwick, Orlov, and others),[5–9] and also of the great practical importance of grain-boundary dissolution. In the representation of high-angle GB, regions of bad and good coincidence have been described[10] by various models: the coincident block lattice (CBL), the grain boundary displacement lattice (GDL), and the full overlap lattice (FOL). Grain boundaries are not a layer of amorphous material, and they can be modelled by the coincident block lattice structure with appropriate parameters.[11]

In the CBL model the grain boundaries are classified as general or special. A special GB in this model has a well defined period, characterised by the reciprocal bulk density of the coincident blocks (Σ). In body-centred (BCC) and in face-centred cubic crystals (f.c.c.) a distinction is made[10] between low-energy ($\Sigma = 3, 9, 11, 17, 27,$ and 33) and high-energy GB (Σ = 5, 7, 13, and 15). The structural model of the GB can be approximated by the model of close packed structural units (Voronyi polyhedra).

Body-centred polyhedra form vacancy-saturated loose regions in the crystal when linked. Boundaries of a general type are adequately described by the structural units model, and they include regions with a periodic structure separated by grain-boundary dislocations. In the presence of external stimuli point defects and line defects are always formed on polycrystals. Subgrain low-angle boundaries are assumed to consist of dislocation networks. There are substantial differences between the dissolution mechanisms of low-angle boundaries and of grain boundaries.

The object of the present review is to analyse the results of studies of the effect of internal boundaries in polycrystals on the phase interaction processes at metal–electrolyte contacts. The need to review these data arose because of the appearance of new models of the dissolution of GB, and of the availability of reliable experimental results on the chemistry of GB and of phase interfaces.

G V Khaldeev A M Gorky Perm State University, 15 ul. Bukireva, 614 600 Perm, Russian Federation. Fax (7-3422) 33 80 14

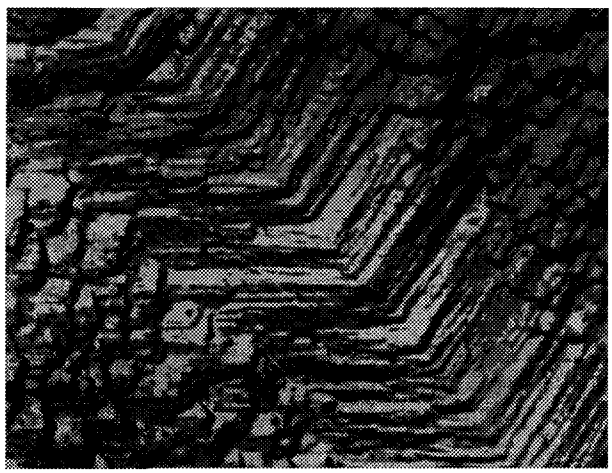
Received 19 August 1994
Uspekhi Khimii **63** (12) 1044–1063 (1994); translated by J I Carasso

II. Dissolution and adsorption of surface-active impurities on low-angle boundaries and on grain boundaries

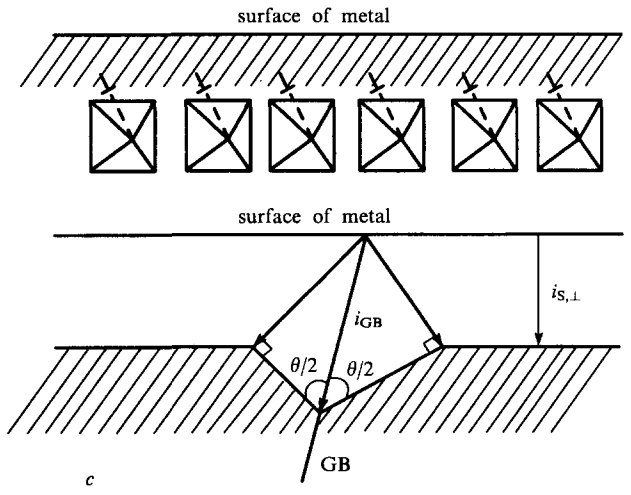
Subsurface dislocations induce the formation of three-dimensional clusters on the crystal surface, which inhibit the action of impurities. Dislocation planes arranged as elastic networks form low-angle boundaries with a misorientation angle $\theta = 2\arcsin(\boldsymbol{b}/2l_d)$, where $\boldsymbol{b}$ is the Burgers vector and l_d is the distance between dislocations. The internal fractal structure of these dislocation networks can be seen on the surface of the crystal as a group of dislocation etch pits (EP) (Fig. 1*a*), the distance between etch pits being an approximate measure of the parameter l_d, from which the misorientation angle θ can be determined. A new phase formed on low-angle boundaries is accommodated in the structure with a specific fractal dimensionality. The dissolution on grain-boundary dislocations for which $l_d > 2\boldsymbol{b}$ is described within the theory developed, for example, in Refs 4 and 12. If the grain-boundary dislocations merge together and lose their individuality, etch grooves are formed on the GB (Fig. 1*b*). The dissolution follows different paths on interblock low-angle ($\theta < 3°-5°$) and high-angle boundaries ($\theta > 15°$) (Fig. 1*c*).



a



b



c

Figure 1. Dissolution on a low-angle boundary (*a*) and the boundary of nickel grains (*b*) (× 12 000) together with a schematic illustration of the grain-boundary dissolution (*c*).

A model of the dissolution on high-angle GB in the simplest form (but corresponding to experimental observations) can be constructed as follows.[13,14] In a pure (>99.99%) bicrystal dissolution along a GB (see Fig. 1*b*) takes place as a result of the generation of dissolution steps whose density depends on the angle θ. The relationship between the dissolution rate (or current) along the plane of the grain boundary i_{GB} and the dissolution rate (or current) normal to the metal surface $i_{S,\perp}$ (see Fig. 1*c*) is the following:

$$\frac{i_{GB}}{i_{S,\perp}} = \frac{1}{\sin(\theta/2)} , \tag{1}$$

$$\Delta i = i_{GB} - i_{S,\perp} = a_S + b_S i_{S,\perp} , \tag{2}$$

for $\lim i_{GB} \to \infty$, $\dfrac{i_{GB}}{i_{S,\perp}} = \dfrac{1}{\sin(\theta_0/2)}$ and $b_S = \dfrac{1}{\sin(\theta_0/2)} - 1$,

for $\lim i_{S,\perp} \to 0$, $i_{GB} \to i_{GB,0}$ and $a_S = i_{GB} = i_{GB,0}$.

Here θ and i_{GB} are the limiting angle and the grain-boundary current, independent of the dissolution of the bulk of the grain, i.e. they are the characteristic parameters of the grain-boundary dissolution.

In the absence of passivation of the grain surface, the rate (or current) of the dissolution on a GB is described by the Marcus formula

$$i_{GB} = i_{GB,0} + \frac{1}{\sin(\theta_0/2)} i_{S,\perp} . \tag{3}$$

By use of the fundamental kinetic equation for the electrochemical dissolution current, Eqn (3) can be expressed in terms of experimentally determined electrochemical parameters. We shall write the Marcus formula[15] as

$$i = K\frac{k_B}{h_p}\frac{Tz^{\neq}}{z}a_0^0 \exp\frac{-\Delta\bar{G}^{\neq}}{RT}\exp\frac{\alpha F\Phi}{RT}\exp\frac{(a-n)F\Phi_1}{RT} , \tag{4}$$

where K is the rate constant for the reaction, $(k_BT/h_p)^{-1}$ is the lifetime of the activated complex (Ac) between the adparticle and a surface atom of the metal (and k_B is Boltzmann's constant), $z^{\neq}$ and z are the partition functions referred to unit volume of the AC and of the reactants in the electrolyte, a_0^0 is the activity of the AC, $\Delta G^{\neq}$ is the nonelectric part of the free energy of activation at low coverages of the metal surface by adparticles, F is the Faraday, Φ is the electron work function, n is the valency of the Ox species in solution, a is the transfer coefficient of the electrode reaction, and Φ_1 is the potential step in the diffuse part of the electrical double layer (EDL).

We simplify Eqn (4) to

$$i = Kc\exp\frac{-[\alpha F(\Phi - \Phi_1) + nF\Phi_1]}{RT} . \tag{5}$$

Here $c = (k_B T_{Z^*}/h_p x) a_0^0 \exp(-\Delta\bar{G}^{\neq}/RT)$ is a term corresponding to the formation of active centres (Ac) on the surface; $(\Phi - \Phi_1)$ is the potential of the electrode relative to the outer coating of the Helmholtz reaction layer. By using formulae (4) and (5), the expression (1) can be converted into

$$\frac{i_{GB}}{i_{S,\perp}} = \frac{K_{GB}}{K_{S,\perp}} \frac{c_{GB}}{c_{S,\perp}} \frac{\exp\{-[\alpha F(\Phi - \Phi_1) + nFF_1]/RT\}_{GB}}{\exp\{-[\alpha F(\Phi - \Phi_1) + nFF_1]/RT\}_{GB}}$$

$$= \frac{1}{\sin(\theta/2)} = \frac{c_{GB}}{c_{S,\perp}} . \quad (6)$$

At high current densities ($i_{S,\perp} \to \infty$):

$$\frac{c_{GB}}{c_{S,\perp}} \to \exp\frac{-\Delta_{GB}(\Delta\bar{G}_0^{\neq})}{RT} = \frac{1}{\sin(\theta/2)} , \quad (7)$$

where $\Delta_{GB}(\Delta\bar{G}_0^{\neq}) = \Delta\bar{G}_{0,GB}^{\neq} - \Delta G_{0,S,\perp}^{\neq}$ is the difference between the energies of formation of the Ac on the grain boundary and on the bulk of the grain. For example, this difference, determined for the Ni/1 M H_2SO_4 system at 298 K, was 32 mJ m^{-2} for a GB with $\theta = 104°$. The dissolution current on the GB, independent of the corrosion current in the bulk of the grain [the first term in formula (3)], is determined by the expression

$$i_{GB,0} = a_{GB}^* i_{0,S,\perp} \exp\frac{-\Delta_{GB}(\Delta\bar{G}^{\neq})}{RT} , \quad (8)$$

where a_{GB}^* is the activity of the surface-active centres distributed over the GB (from the physical point of view it is the surface activity of the grain-boundary dislocations). The trapped lattice dislocations increase the energy of the GB by an amount equal to the elastic field of the dislocations:[16]

$$\Delta E \cong \frac{G_c b^2}{4\pi(1-\nu)2l_d} \ln\frac{e\alpha l_d}{\pi b} , \quad (9)$$

where G_c is the shear modulus, ν is Poisson's ratio, e is the base of natural logarithms, α (= 1–2) is the energy parameter of the dislocation core, and l_d is the distance from the dislocation to the surface. For a given polycrystal, the parameter ΔE depends also on Σ and θ. The corrosion activity of the GB in very pure polycrystals varies periodically with the number of dislocations absorbed (ρ_d) and with the misorientation angle (θ), thus influencing the adsorption properties of both the GB themselves and the adjacent grain-boundary volumes.

The adsorption properties of the grain-boundary volumes affect the dissolution process. The adsorption on the GB is examined both 'from inside' (from the bulk of the grain) and 'from above' (from the interface). The adsorption 'from inside' is produced by the diffusional inflow of impurities on the GB and obeys the expression

$$\frac{c(t) - c_0}{c_\infty - c_0} = 1 - \exp\frac{-4Dt}{(\Delta\gamma^{\neq})^2 d^2} \operatorname{erfc}\frac{2(Dt)^{1/2}}{d\Delta\gamma^{\neq}} , \quad (10)$$

where $c(t)$ is the concentration of impurities on the GB at time t, c_0 and c_∞ are the initial and the equilibrium concentration of impurities on the GB, $\Delta\gamma^{\neq} \cong (\exp \Delta H)/k_B T$ is the supersaturation, ΔH is the enthalpy of the GB–impurity bond, D is the coefficient of diffusion of the impurity in the crystal, and d is the thickness of the GB. For hydrogen $D_H = 1 \times 10^{-8} - 1 \times 10^{-9}$ m^2 s^{-1} and $\Delta H = 10-60$ kJ mol^{-1}. Deformation of the polycrystal can induce the accumulation of impurities on the GB by dislocational transport.[17] Moving dislocations adsorb the impurities and transport them over the GB. The dislocational permeability of the GB is determined by the angle θ, and the chemical properties of the GB vary accordingly.

The equilibrium segregation of the impurities (added atoms or originally present impurities) on the GB can be described[17] by the Fermi–Dirac distribution

$$c = c_{0,L} \exp\frac{\Delta G_a}{RT}\left(1 + c_{0,L}\exp\frac{\Delta G_a}{RT}\right)^{-1} = c_0 \exp\frac{\Delta H}{RT} , \quad (11)$$

where $c_{0,L}$ is the equilibrium concentration in the solution and ΔG_a is the difference in free energy between the additives dissolved in the GB and in the crystal lattice. The enthalpy ΔH of the bond between the grain-boundary surface and the surface-active impurity species (similar in size to the atoms of the crystal) is in the range of 150–200 kJ mol^{-1} for the 3d metals. The adsorption on the GB can be calculated by using the Gibbs concepts of reversible adsorption and of the decrease in the surface tension of the grain boundaries produced by the creation of a surface excess. According to the Gibbs formula

$$d\gamma = Vdp - SdT - \sum_i \Gamma_i d\mu_i \quad (i = K^+, A^-, M^{n+}, e^-) , \quad (12)$$

where V and S are, respectively, the volume and the entropy of the adsorbed layer of the quasicrystalline phase of surface-active substance, Γ_i is the coverage of the metal surface by particles of the ith kind (Gibbs adsorption), $\mu_i = k_B T \ln c(x) + E(x) + \text{const}$ is the chemical potential of the ith species, $E(x)$ is the energy of the attractor, $\mu_0 \equiv E(x) + \text{const}$, K^+ and A^- are the cation and the anion of the supporting electrolyte, M^{n+} is the charged metal ion, and e^- is the electron. By using the Gibbs formula and the distribution (11) we can obtain an expression for the decrease in surface tension:

$$\Delta\gamma = \gamma_{GB} - \gamma_B = RT\,\theta_{GB} \ln\left(1 + c_0 \exp\frac{\Delta G_a}{RT}\right) . \quad (13)$$

Here γ_B is the absolute energy of formation of the GB, θ_{GB} is the coverage of the GB by impurity particles, and c_0 is the background concentration. The decrease in γ_{GB} is used to calculate $\Delta G_a = \Delta E_a - T\Delta S_a$, where ΔE_a and ΔS_a are the energy and the entropy change of the interaction of the surface-active impurity with the GB. Under equilibrium conditions the chemical potentials of the ith species (SAS particles) on the free metal surface (μ_S), on the grain boundary (μ_{GB}), and in the solution (μ_B) are identical.

In the interpretation formulated by McLean and Hondros[18] we require a knowledge of the dependence of the surface tension γ_{GB} of the grain boundary on the surface concentration of the adsorbate in order to determine the adsorption:

$$\gamma_{GB} - \gamma_B = -T\Delta S_a - \sum_i \Gamma_i \mu_i . \quad (14)$$

Here the coverage $\Gamma_i = -[\partial\gamma/\partial\mu_i]_{T,\mu_{j\neq i}}$ is a crystallographically determined quantity, because neighbouring grains are differently oriented and the adsorption of the SAS impurity on them is different. The Gibbs equation in the form (12) can be used to calculate Γ_i for the components from the known isotherms of the surface tension γ_{GB} and of the chemical potential μ_i of the components in the grain.[18] For a two-component system

$$d\gamma = -\Gamma_1 d\mu_1 - \Gamma_2 d\mu_2 = -\frac{\Gamma_2 d\mu_2}{1-c} , \quad (15)$$

where c is the concentration of the SAS impurity.

In order to determine the adsorption accurately, we need to know the activity a of the components rather than their concentration c and to find the chemical potential of the adsorbed SAS.

In the theoretical description of the adsorption on polycrystals in terms of the lattice models we can use an approach developed for the analysis of stresses in Somigliana dislocations. In this case the adsorption properties on the grain boundaries and on their bulk should have their equilibrium values, and should be continuous at all points. The problem can be solved by the nonlinear theory of elasticity.[18]

The differences between adsorption–desorption processes on the surface of crystals and on the grain boundaries can be studied experimentally by comparing the electrochemical characteristics of monocrystals and polycrystals. A very instructive example of this approach is provided by the study of the anodic oxidation of CO on mono- and on polycrystalline Pt electrodes in 0.05 M $HClO_4$. At low overvoltages ($\eta < 0.1$ V), the adsorption is described by the Langmuir isotherm, is independent of the grain size and of the pH of the solution, and takes place according to the scheme

$$Pt(CO)_{ads} + H_2O \longleftrightarrow Pt(COOH)_{ads} + H^+ + e^-.$$

Increasing the overvoltage (to $\eta > 0.2$ V) and the concentration of active centres (by changing from single crystals to polycrystals) affects the final products. In the bulk of the grain boundaries, the electrochemical process follows a different path:

$$Pt(CO)_{ads} + OH^- \longleftrightarrow Pt(COOH)_{ads} + e^-,$$

$$Pt(CO)_{ads} + 3OH^- \longleftrightarrow Pt + CO_3^{2-} + 2H_2O + e^-.$$

On a platinum polycrystal with a small grain size (~ 1 μm) and a correspondingly large spread of GB, the formation of carbon dioxide becomes possible at high anodic potentials ($E > 1.4$ V):

$$Pt(CO)_{ads} + H_2O \longleftrightarrow Pt + CO_2 + 2H^+ + 2e^-.$$

Anodic polarisation in the high positive range of potentials ($E \gg 1.4$ V) activates the grain-boundary volumes in the metal. Even more complex reactions are possible (according to steric considerations) on extended defects of the GB surface: for example

$$CH_2\text{—}CH(CH_2)_8CO_2H + 4H_2O \longrightarrow$$

(Pt)

$$\longrightarrow Pt + H_3C(CH_2)_7CO_2H + 2CO_2 + 11H^+ + 11e^-.$$

The nature of this substantial change in the chemical path of the reactions reflects the difference in structure and in chemical composition between the grain-boundary volumes and the bulk of the grain. The polyhedral structure of the GB provides ready-made elements for the formation of surface clusters. The pores and the polyhedra of the GB in the 3*d* metals can be filled relatively easily with impurity elements (Ru, Os, Rh, Ir). Impurities which lower γ and favour the formation of GB with the most stable structure are usually concentrated on the GB: in most cases these are chalcophilic elements. Reactions taking place relatively easily on the GB include impurity precipitation and carbide formation, which lower the concentration of elements with a high oxygen affinity.

III. Distribution of dislocations in near-surface layers of crystals

Many physical, mechanical, and corrosion-electrochemical properties of polycrystalline metals depend on the distribution of dislocations (DD) near the internal boundaries. The DD process is statistically independent.[20] However, within the crystallites (and especially in the region of subgrain boundaries and of grain boundaries), DD in the form of planar aggregates are fairly often seen. An edge dislocation does not interact strongly with a low-angle dislocation boundary,[21] and when the slip plane of the edge dislocation is perpendicular to the wall the interaction is completely suppressed. On the other hand, high-angle GB act as dislocation stoppers, which cannot be surmounted by thermal activation. However, the long-range interaction of the dislocations with the GB is quite weak, as in the case of the low-angle boundaries.

The effect of the dislocation density ρ_d on the electrochemical behaviour of crystals in electrolytes has been studied intensively[22,23] in the context of confirming the Rebinder and Ioffe effects on the physicomechanical properties of crystals caused by exposure of the crystal surfaces to the components of liquid condensed media. The 'skin-deep' aggregation of dislocations in the near-surface layer is due essentially to the action of image forces, whose energy (in the framework of the linear theory of elasticity) is given by

$$E_u = \beta G_c \boldsymbol{b} \ln \frac{2l_d}{\boldsymbol{b}} . \tag{16}$$

In this case, $\beta = 1 - \nu$ for edge dislocations and $\beta = 1$ for screw dislocations; l_d is the distance from the dislocation to the surface. At a high level of relaxation of the near-surface layer of the crystal (i.e. for a change in the lattice constant of more than 10%) the inner electric double layer of the metal stops the 'floating' dislocation.[4] The dislocation distributions in the near-surface layer depend first of all on the type of crystal and on the nature of previous mechanical treatments. In an ultra-thin surface layer of the crystal, the parameter ρ_d can decrease (Fig. 2). In the case of rectilinear edge dislocations,[23] the distribution as a function of depth z can be calculated by using the formula

$$\rho_{d,z} \approx \frac{L}{z} \exp \frac{-E_{d,z}}{Lzk_BT} , \tag{17}$$

where L is the length of the dislocation (< 1 μm), and $E_{d,z}$ is the energy of the dislocation. For dislocation half-loops, the distribution takes the form

$$\rho_{d,z} \sim \frac{A}{z} \exp \frac{-B \ln z}{z} . \tag{18}$$

Here $A = G_c \boldsymbol{b}^2 / 2\beta$ (G_c is the shear modulus) and B is the attenuation coefficient of sound in the crystal.

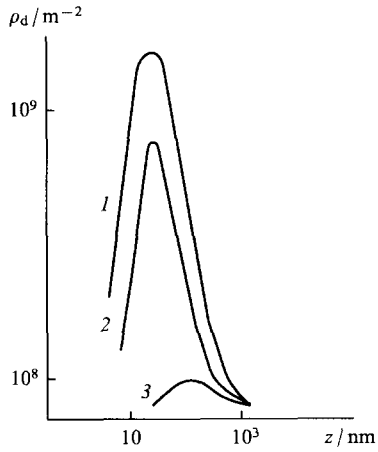


Figure 2. Distribution of rectilinear edge dislocation as a function of the depth of the near-surface layer (z) in copper (curve *1*), nickel (curve *2*), and silicon (curve *3*) crystals.

The distance from the crystal surface, where the density of dislocations $\rho_{d,z}$ is a maximum, can be determined from the condition $\partial \rho_{d,z} / \boldsymbol{b} z = 0$:

$$z_{max} \equiv \frac{G_c \boldsymbol{b}^3}{4\pi(1-\nu)} (k_BT)^{-1} , \tag{19}$$

where ν is Poisson's ratio.

The aggregation of edge dislocations in the near-surface layer of the metal is caused by thermoelastic stress effects. The analytic solution of the equilibrium distribution problem for rigid parallel rectilinear dislocations on the slip plane has been obtained [24, 25] on the assumption of a continuous distribution for a periodic potential of the external forces $U(x)$. The x axis is perpendicular to the dislocation lines and corresponds to the slip direction. The equilibrium DD in the field of $U(x)$ (the potential energy for a unit length positive dislocation) is determined in this case by a function of their linear density $\rho_d(x)$ which can be expressed [16] as a Fourier series:

$$\rho_d(x) = \sum_{k=-\infty}^{+\infty} \rho_{d,k} \exp(ia_k x) \quad . \tag{20}$$

Here

$$\rho_{dd,k} = -\frac{2\pi|k|U_k}{|A|} \quad \text{for } k \neq 0 \quad (\rho_0 \text{ is arbitrary}),$$

$$U_k = \frac{1}{l}\int_{-l/2}^{+l/2} U(x)\exp(-ia_k x)\mathrm{d}x \quad , \tag{21}$$

$a_k = 2\pi k/l$ [l is the period of $U(x)$ and of $\rho(x)$].

Grain sub-boundaries and boundaries are characterised by local minima in the potential energy $U(x)$. Then, having calculated the DD for the self-repeating potential wells, we can describe the changes in ρ_d in the bicrystal. Fig. 3 shows the result of a computer calculation allowing for 40 harmonics ($-20 \leqslant k \leqslant 20$) in the representation of the $U(x)$ profile. In this case, the potential well has very steep walls, and therefore the emission of dislocations from this well and the surmounting of this obstacle are seriously hindered. However, outside the limits of the potential well $U(x)$ = const, and there is no elastic long-range interaction between the dislocations and this obstacle. The mid-point of one of the internal boundaries in the bicrystal was used as the origin for the measurements. The distribution of the dislocations is given within a single period of $\rho_d(x)$. As could have been expected, on the GB ρ_d is higher than the average level, but (conversely) the regions immediately adjacent to the boundary have a ρ_d value well below the average.

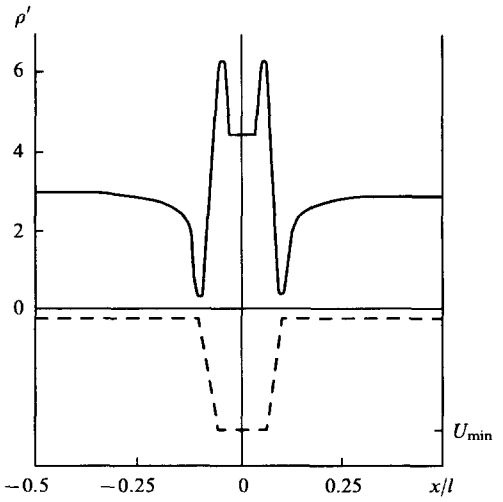


Figure 3. Distribution of dislocations in the field of repeated potential wells:

$$\rho' = \frac{Al}{2\pi|U_{min}|}\rho, \quad \rho = \frac{6\pi|U_{min}|}{Al} \quad .$$

An experimental determination of the DD near a grain boundary [misorientation angle of the grains θ = 13°–15°, for which expressions (17)–(20) are applicable] was carried out for pure iron (99.99%, $\rho_d = 2.0 \times 10^{11}$ m^{-2}). Selective electrochemical etching in the passive region of potential was applied in a 1 M solution of H_2SO_4 (290 K, E = 0.80 V, t = 300 s). Under these etching conditions, the nondislocated part of the crystal surface is passivated by oxides, and dissolution takes place only on the defects.

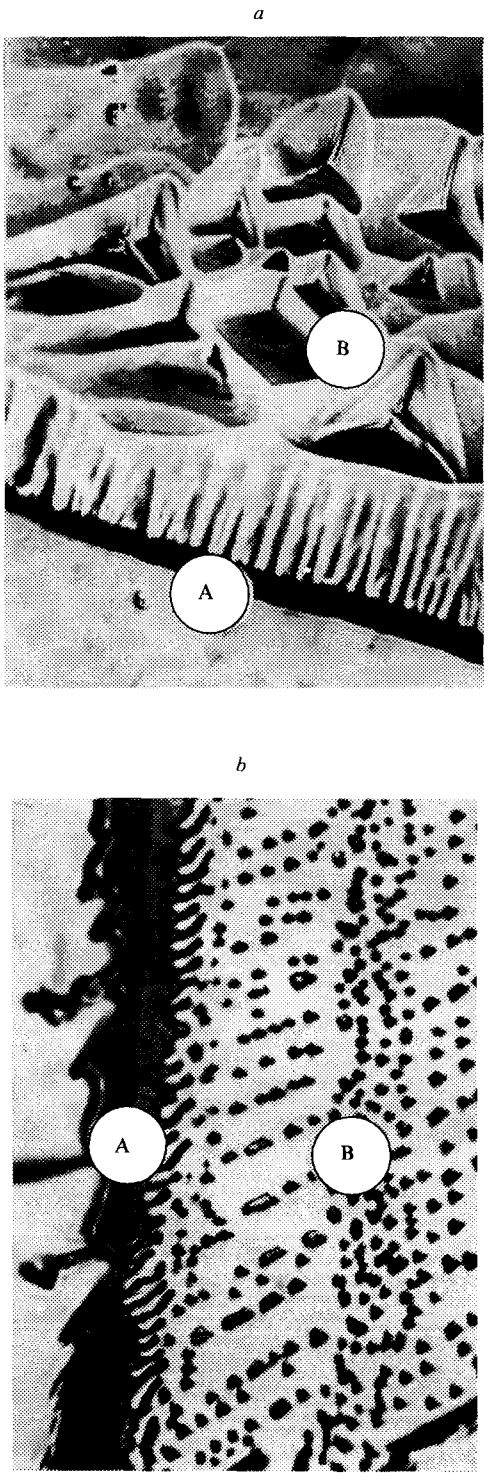


Figure 4. Electrochemical (*a*) and thermal (*b*) etching of zone-purified iron (× 960). A—grain-boundary; B—EP zone.

Etch pits (EP) are formed on the Fe(111) surface both in the region of the GB (Fig. 4*a*, region A) and at some distance from it (region B); there is a fairly wide 'dead' zone directly adjacent to the GB where no etch pits are found. The presence of a similar zone on the Fe(110) face is observed only after a hydrogen anneal of the iron ($p = 6 - 10^{-3}$ Pa, 1173 K, $t = 3.6 \times 10^3$ s) by the method of thermal EPs, which are formed because of the selective oxidation of the dislocation outcrops on the crystal surface (Fig. 4*b*). The size of the dislocation-free regions is 7–12 μm. We should note that thermal oxidation (unlike electrochemical etching) does not produce EP in the region of the boundaries.

The density of dislocations on the GB is higher than the average level, but in the region directly adjacent to the boundary it is anomalously low. This effect has stimulated the interest of experimental workers, and it has been carefully analysed[26] by high-resolution transmission electron microscopy methods. The width of the dislocation-free regions for GB with small Σ values was found to be ~15 μm. The localisation of the dissolution process on a defect has a protective action on the corrosion of the dislocation-free region. When polycrystals are exposed to corrosion-electrochemical interactions the selective dissolution of the dislocation outcrops results in the appearance of wide nonetched regions.

The distribution of ρ_d directly influences the rate of corrosion i_{cor}, which is low during the initial period of exposure but becomes stable after going through a maximum.[27]

The effect of corrosion-active media on the surface energy (which is stronger on the γ_{GB}) should be mentioned, in addition to the image forces and the thermoelastic stresses, as one of the physicochemical reasons for the accumulation of dislocations in the near-surface layer.

Extensive reports on the search for quantitative estimates of the effect of the dislocation density ρ_d on the dissolution of metals have been published. The change in the kinetic parameters of the anodic dissolution of iron in acid media produced by heat treatment is usually ascribed to a decrease in ρ_d. The intermediate $(FeOH)_{ads}$, chemisorbed on the iron atoms in a dislocation pipe $Fe(FeOH)_{ads}$ and which is able to catalyse the dissolution process,[28] is formed on the dislocations. These effects have been noted also on other transition metals (for example, nickel[29]). On deformed nickel ($\varepsilon > 10\%$) with a high density of dislocations, the adsorption of water dipoles in solutions of $Na_2SO_4 + (C_2H_5OH$, C_4H_9OH, $C_6H_{13}OH)$ blocks the AC (dislocation outcrops), and the dependence of the double-layer capacity c_{DL} on the electrode potential E (measured by a pulsed galvanostatic method) does not differ significantly from the background value. After annealing a nickel electrode (973 K, $t = 5.4 \times 10^3$ s), with a corresponding decrease in the spread of the GB and in ρ_d, we observe a decrease in c_{DL}. Adding to the solution substances with a high specific adsorption activity [$SC(NH_2)_2$, $(CH_3)_2CO$, C_3H_7COOH] produces changes in ρ_d which only marginally affect the $c_{DL} - E$ curves.

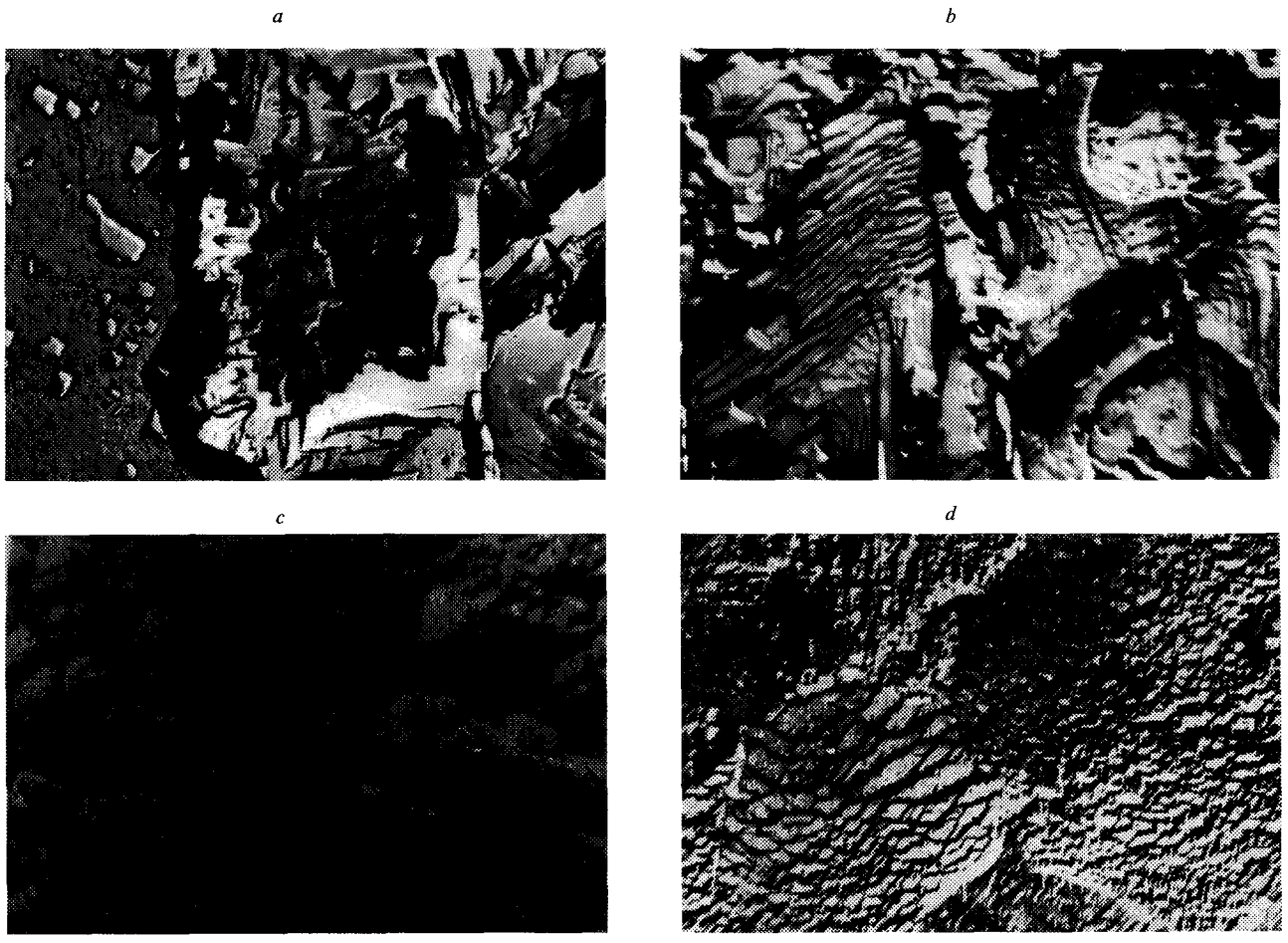


Figure 5. Morphology of the surfaces of dissolving iron (*a*), nickel (*b*), copper (*c*), and tungsten (*d*) polycrystals at the current oscillation potentials (× 12000).

IV. Current and potential oscillations during grain-boundary dissolution

On grain-boundary volumes the processes of dezincification (brass, bronze, Cu–Zn alloys) and of selective dissolution of stainless steels [30] and of other metals follow different paths. The oscillations of the anode current i_a at potentials more positive than the Flade potential E_{Fl} on the anodic polarisation curve are usually attributed [31,32] to an enhanced grain-boundary dissolution. A metallographic analysis of the surface of samples held for short times (t = 20–30 s) at different current oscillation potentials in the anodic region showed that grain-boundary volumes in polycrystals dissolve rapidly (Fig. 5). In many experimental studies it was assumed that the current oscillations were apparatus artefacts, and the oscillations were excluded from the $E-i_a$ curves. The enhanced adsorption activity of the GB allows us to control the current oscillations by introducing surfactants into the electrolyte. [4] Thus, the current oscillations on a nickel electrode can be suppressed by adding corrosion inhibitors to the solution [for example, n-octylphenylmethanesulfonate]. However, substances which act as corrosion inhibitors on annealed polycrystals may not have the same effect on elastically stressed metals (ε < 5%). The amplitude of the current oscillations on elastically stressed metals is higher, and the potential region which produces oscillations is wider, than in the case of annealed metals. Thus anthraquinone derivatives, which inhibit the acid corrosion of titanium and of stainless steels, accelerate the intercrystallite corrosion of stressed 12X18N9T stainless steel. [33]

The current (or potential) oscillations in potentiostatic (or galvanostatic) circuits are well known electrochemical effects, first reported by Fechner in 1928. Near the Flade potential E_{Fl} on the $E-i_a$ curve, we observe an electric instability whose amplitude decreases at more noble potentials (Fig. 6*a*). Early explanations of this effect relied on the assumption of a periodic transition of the metal from a passive into an active state. [32] On polycrystals of the transition metals, these activation regions should be found on grain boundaries. The diagnostic criterion of the instability (current oscillations) is provided by the appearance on the $E-i_a$ polarisation curves of regions with a negative slope $di(E)/dE(i) < 0$ (Fig. 6*b*). In accordance with the ideas of catastrophe theory, [35] this suggests the existence of three fluxes of particles with different i_a values for E = const.

Current oscillations associated with periodic passivation–repassivation reactions on the surfaces (mainly on the bulk of grain boundaries) of porous oxides have been explained as follows. The passivation–repassivation process alters the porosity of the passivating oxide films, $\varphi = f(\theta_{Ox})$, where θ_{Ox} is the coverage of the surface by the oxide phase (the accessibility of the metal surface to the electrolyte). The average rate of flow of the electrolyte $\bar{v}$ depends on the pressure p:

$$\bar{v} = -\Pi_i(\varphi)\,\nabla p \ ,$$

where Π_i is the permeability of the oxide layer. Ortoleva's model [36] assumes that an impenetrable oxide structure is more likely to be formed on a GB, and that the bulk of the grain has a porous oxide layer permeable to ions. Treating this layer as a structure consisting of n pores of volume L^3 and an insoluble oxide with a volume fraction $1-N_f$ gives the expression

$$\varphi + nL^3 = N_f \ . \tag{22}$$

The changes in porosity with time will be determined by the kinetics of the formation of pores in the oxide structure:

$$\frac{\partial\varphi}{\partial t} = -n\frac{\partial L^3}{\partial t} \ . \tag{23}$$

For the rate of growth of the oxide islets on the GB in two-dimensional coordinates, we can write

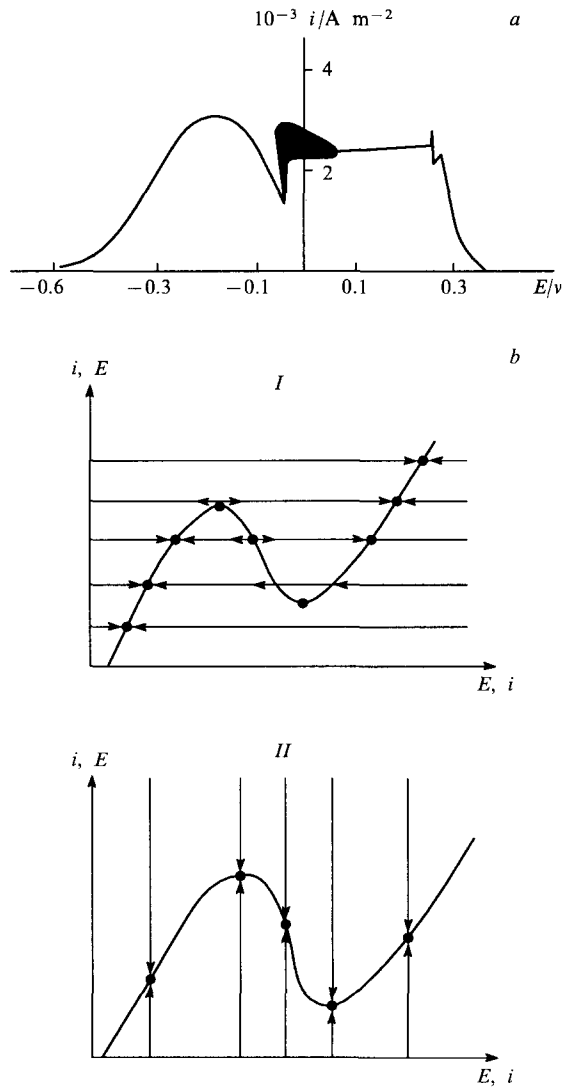


Figure 6. Polarisation curve (*a*) for the Fe–1 M H_2SO_4 system (V_E = 0.005 V s^{-1}) with a current oscillation section. The schematic illustration of the polarisation measurement (*b*) explains the appearance of sections with a negative slope on the $E-i$ curves.

$$\frac{\partial L^3}{\partial t} = KL^2[c(t) - c_0] \ , \tag{24}$$

where K is the rate constant for the growth of oxide, and c_0 and $c(t)$ are respectively, the equilibrium (in solution) and the time-dependent concentrations of the M^{n+} ions in the pore. From Eqns (22)–(24), we obtain

$$\frac{\partial\varphi}{\partial t} = -Kn^{-1/3}(N_f - \varphi)^{2/3}[c(t) - c_0] \ .$$

If the density of the electrolyte is independent of $c(t)$ and p, the law of energy conservation can be written in the form

$$\frac{\partial\varphi}{\partial t} = -\nabla\,[\varphi\chi(\varphi)\,\nabla p] \ ,$$

whereas for the dissolving metal we have

$$\frac{\partial\varphi}{\partial t} = \nabla[\varphi\Delta(\varphi)\,\nabla c(t) + \varphi c(t)\chi(\varphi)\,\nabla p] + \rho\frac{\partial\varphi}{\partial t} \ . \tag{25}$$

Here the diffusion coefficient $\Delta(\varphi)$ and the electric conductivity $\chi(\varphi)$ depend on the porosity (ρ is the density of the metal). An analysis of the solution of Eqn (25) shows that under the conditions of current and potential oscillations, the front of the moving phase boundary is unstable if it is planar.

The instability problem has a strong relevance to the processes responsible for the dissolution of polycrystalline metals. On the surface, we find regions (the GB and the bulk of the grain) comparable in area and in their relative contribution to the formation of a flux of dissolving matter. The specific flux of M^{n+} ions on the GB can be several orders of magnitude greater than the corresponding flux from the surface of the grain. At the same time the adsorption activity of the GB is also very much greater. If the electrolyte contains easily adsorbed components, these are redistributed on the surface during the dissolution of the crystal. This produces opposing transport effects through the fluxes of M^{n+} from the metal and to the metal on the phase boundary.

Current oscillations can be explained by a retardation (and acceleration) of the motion of the dissolution steps [37] as well as by the activation–passivation of the grain-boundary volumes. On an iron electrode in 0.5–1.0 M H_2SO_4, the salt $FeSO_4$ (in a colloidal state near the electrode surface) acts as a reversibly passivating reagent. The formation of oxides, hydroxides, and salts with a structure and properties varying as a function of the heterogeneity of the electrode surface is the basis of the most significant concepts regarding the current (or potential) oscillation phenomena. In the layer nearest to the electrode clusters of particles can be formed and have a stable existence. [38] Upon landing on the electrode surface, they settle on the steps and block their motion. The retardation mechanism is similar to that proposed by Khaldeev and Kamelin: [39,40] the aggregation of foreign particles into Toda chains, which block the motion of the surface dislocations.

In the oscillatory potential model, [41] it is assumed that the growth and dissolution of passive films are complicated by the transfer of H^+ ions between the electrode surface and the solution. This destabilises the passivation potential E_n and the Flade potential E_{Fl}. The oscillation process can be divided into the following stages:

(1) $E_n < E_{Fl}$; the electrode surface is activated, the metal dissolves, the current is limited by the transfer of the H^+ ions (whose concentration decreases in the neighbourhood of the surface);

(2) the parameter E_{Fl} is determined by the concentration of H^+ ions [$E_{Fl} \sim F(c_{H^+})$], which decreases during the first stage, so that the Flade potential also decreases: $E_{Fl} < E_n$;

(3) a passive film having a much lower rate of dissolution is formed;

(4) the E_{Fl} value increases as a result of the third stage, and $E_n < E_{Fl}$;

(5) the oxide film dissolves.

These cycles can be repeated indefinitely.

The kinetics of the process can be expressed as follows:

$$\frac{dE}{dt} = K_1 - K_2 - K_3\theta_{Ox} + K_4 E W(E, \theta_{Ox}) \ , \tag{26}$$

$$\frac{d\theta_{Ox}}{dt} = K_5 E W(E, \theta_{Ox}) \ , \tag{27}$$

where $E = E_n - E_{Fl}$ is the time-dependent potential; θ_{Ox} is the coverage (the passivated part of the surface). The rate constants for all the stages of the oscillatory process ($K_2 - K_5$) are positive. The function $W(E, \theta_{Ox})$, which normalises the coverage, is defined as follows:

$$W(E,\theta_{Ox}) = \theta_{Ox} + (1 - 2\theta_{Ox})U(E) \ , \tag{28}$$

where $U(E)$ is the Heaviside function. Therefore we can write

$$W(E,\theta_{Ox}) = \begin{cases} 1-\theta_{Ox} & \text{for } E > 0 \ , \\ \theta_{Ox} & \text{for } E < 0 \ . \end{cases}$$

Perlstein and Johnson [42] introduced the symbols $V = K_5E/K_2$ and $\tau = kt$ and put expressions (26) and (27) in the form

$$\frac{dV}{dt} = bh - V - b\theta_{Ox} + \frac{VG(V, \theta_{Ox})}{c} \ , \tag{29a}$$

$$\frac{d\theta_{Ox}}{dt} = VG(V, \theta_{Ox}) \ , \tag{29b}$$

and he replaced Eqn (28) by the normalised function

$$G(V,\theta_{Ox}) = \theta_{Ox} + (1 + 2\theta_{Ox})U(V) \ , \tag{30}$$

where $b = K_3K_5/K_2^2$, $c = K_2/K_4$, and $h = K_1/K_4$ (the quantities b and c are positive).

It follows from the equations given above that unique systems of states can exist:

$$(V,\theta_{Ox}) = \begin{cases} (bh,0) & h \leqslant 0 \\ (0,h) & 0 \leqslant h \leqslant 1 \\ (bh-b,1) & 1 \leqslant h \ . \end{cases}$$

Thus the stable state of the phase boundary is defined by the two parameters b and h.

In a subsequent modification [41] of Eqns (29) and (30), the function G was replaced by G^*, i.e.

$$\frac{dV}{dt} = bh - V - 6\theta_{Ox} + \frac{VG^*(V, \theta_{Ox})}{c} \ , \tag{31a}$$

$$\frac{d\theta_{Ox}}{dt} = VG^*(V, \theta_{Ox}) \ , \tag{31b}$$

$$G^*(V,\theta_{Ox}) = \theta_{Ox} + (1 - 2\theta_{Ox})\chi(V) \ ,$$

$$\chi(V) = 1 - \frac{1}{\exp(AV) + 1} \ ,$$

where A is a constant ($A \gg 0$). The function $\chi(V)$ is a degenerate Heaviside function. For large A, the χ value is close to zero (for negative V) and to 1 (for positive V). However, the function varies (between 0 and 1) near $V = 0$.

A very simple condition for the stable state follows from the modified relations (31);

$$V, \theta_{Ox} = 0, h \ ,$$

i.e. the stable potential V is zero, and a part of the metal surface ($\theta_{S,Ox}$) is passive; the latter is determined by the parameter h. The model is applicable for $0 \leqslant h \leqslant 1$.

An estimate of the potential oscillations can be used to determine the likelihood of depassivation of stainless steel. [43] In a system in which intermediate species are produced and disappear, the oscillations of the potential E are given by bifurcation theory [44] as

$$\frac{dx}{dt} = A - (B + 1)x + x^2 + D\frac{d^2x}{dr^2} \ , \tag{32a}$$

$$\frac{dy}{dt} = Bx - x^2y + QD\frac{d^2y}{dr^2} \ . \tag{32b}$$

Here x, y are real functions of the variables t and r (t is time, r is a spatial coordinate belonging to the segment [0, 1]; A, B, D, Q are positive numbers, where B is the bifurcation parameter. If the flux of particles towards the phase boundary is constant a new cycle begins for $B = 1 + A$. If the concentrations of the particles M_S^{n+} and M_L^{n+} on the two sides of the phase boundary remain constant, the new cycle begins at $B = A + D(1 - Q)$. The solutions $X(0,t) = X(1,t)$, and $XY(0,t) = Y(1,t) = B/A$ are stationary.

V. Intercrystallite corrosion

Etch grooves are formed at the boundary between neighbouring grains of identical chemical composition in a bicrystal (Fig. 7). Mechanical equilibrium is achieved by superposing the interfacial tension forces γ_{SL} and the energy of the internal interfaces γ_{GB}. According to Mullins,[45] the condition for an equilibrium state is

$$\gamma_{GB} = 2\gamma_{SL}\cos\frac{\theta}{2} . \quad (33)$$

Near the etch groove, a ramp is formed (Fig. 7); its profile is given by the condition

$$m = \cot\frac{\theta}{2} . \quad (34)$$

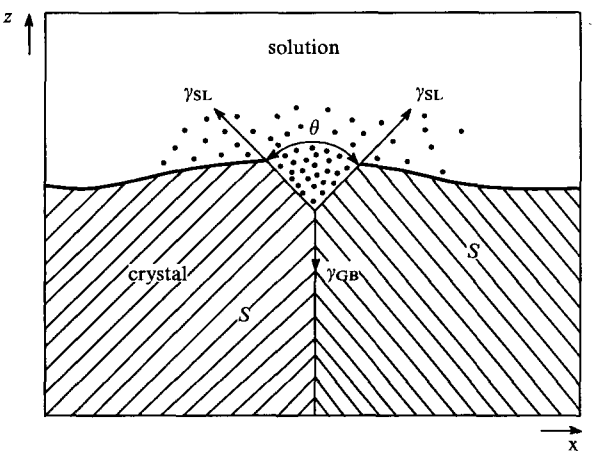


Figure 7. The formation of an etch groove on a metallic bicrystal.

We note that the existence of this profile follows both from the impurity distribution conditions near the GB and from the condition determining the change in the dislocation structure of the crystal near the GB (see Fig. 3). The distribution of impurities along the normal x to the plane of the GB is strongly nonlinear. On the plane of the GB, their concentration is much higher than the equilibrium value: this is followed by a 'dead' zone, after which the concentration suddenly increases.

Along the plane of the GB (i.e. along z), the impurities are distributed according to the relay (cooperative) grain-boundary diffusion mechanism.[46] This model assumes an alternation of grain-boundary barriers (body-centred polyhedra) and of free volumes. Grain-boundary segregations are formed during a preparative stage. In the second stage, the actual grain-boundary diffusion of impurities takes place as a result of a diffusion jump through the barrier and of a concerted displacement within the free (loose) volume. The Gibbs–Thomson relation describes the distribution of the impurity along x:

$$c_S(x,t) = c_\infty\left[1 + \frac{\gamma_{SL}\Omega}{RT}K_M(x,t)\right] . \quad (35)$$

Here c_∞ is the concentration of solution particles on the flat ($K_M = 0$) surface, Ω is the atomic volume of the metal crystal, and $K_M(x,t)$ is the curvature of the metal surface. Mullins[47] modified this model and adapted it to a pure diffusion treatment by introducing three parameters: the distance d between the top of the ramp and the bottom of the groove, the distance d' between the initial flat surface and the ramp, and the distance between the edges W:

$$d = 1.01\,m(A't)^{1/3} , \quad (36a)$$

$$d' = 0.86\,m(A't)^{1/3} , \quad (36b)$$

and

$$W = 5(A't)^{1/3} , \quad (36c)$$

where $A' = (D\gamma_{SL}\Omega^2 c_\infty)/RT$, $t = A't$, and D is the diffusion coefficient of M^{n+} in the crystal. In the case of convective diffusion, the profile (see Fig. 7) may be asymmetric for the different crystals A and B of the bicrystal.[48] In x, y coordinates, the curvature of the metal surface is described by the expression

$$K_M(x,\tau,\alpha) = m(\pi\tau\alpha)^{-1/2}\exp\frac{-x^2}{4\tau\alpha} , \quad (37)$$

and the profile of the surface in the normalised $\eta = x/2\sqrt{\tau\alpha}$ coordinates is

$$\frac{W(\eta)}{2m\sqrt{\tau\alpha}} = -\eta\,\mathrm{erf}(\eta) - \frac{1}{\sqrt{\pi}}\exp(-\eta^2) + \eta = X(\eta) . \quad (38)$$

Here τ is the dimensionless time, $\alpha = Pe/2 = 0.5V/D_A$ (where Pe is the Péclet number, V is the average rate of penetration of A into the A–B bicrystal, and D_A is the diffusion coefficient of A in the A–B bicrystal).

If the diffusion process on the metal surface is markedly influenced by electromigration, the curvature of this surface in the two-dimensional variant (in x, y coordinates) corresponds to the expression[49]

$$K_M(x,\tau,\alpha) = \frac{2g}{1+\beta^{1/3}+\beta^{2/3}}(A_1,t)^{1/3}\sum_{n=0}^{\infty} b_{j,n}\left[\frac{x}{(A_j t)^{1/3}}\right]^n , \quad (39)$$

where $2g$ is the ratio of the free energies of the GB and of the surface per unit surface area, and $\beta = D_A/D_B$ (D_B is the diffusion coefficient of B in the A–B bicrystal), and

$$A_j = \frac{A' z|e^-|\rho i_m}{k_B T} ,$$

where $z|e^-|$ is the effective charge, ρ is the resistance, i_m is the electromigration current density, and $j = 1, 2$. The resulting profile is nonlinear, the maximum amplitude of y being found at $x = 1$.

When the difference in the rates of dissolution between the bulk of the grain and along the GB is large ($i_{GB} \gg i_{S,\perp}$), we can use a model proposed by Peschke et al.[37] and similar to the well known Fischer model, according to which an etch groove with perpendicular walls is formed (Fig. 8*a*). In practice, this state of affairs is typical of the dissolution of hydrogen-saturated polycrystals showing passivation (Figs 8*b* and 8*c*). The local loss of passivity on the GB produces a large increase in i_{GB} in the z direction. The convective diffusion equation

$$v(r)\frac{\partial c(x,t)}{\partial z} = D_A\frac{1}{r}\frac{\partial}{\partial r}\left[r\frac{\partial c(x,t)}{\partial r}\right]$$

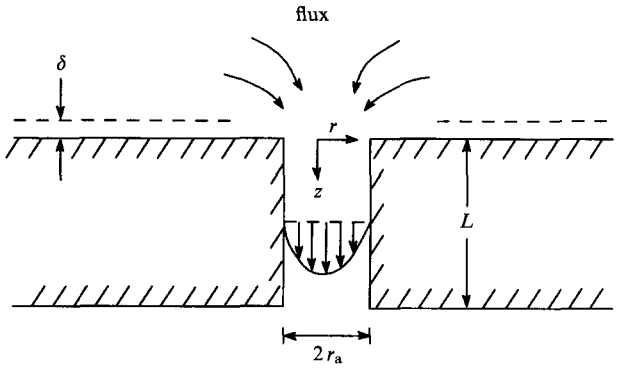
for this situation can be expressed as

$$F(\bar r)\frac{\partial \bar c}{\partial \bar z} = \frac{1}{Pe}\left[\frac{1}{\bar r}\frac{\partial}{\partial \bar r}\left(\bar r\frac{\partial \bar c}{\partial \bar r}\right)\right] , \quad (40)$$

where $F(\bar r)$ is the dimensionless velocity

$$F(\bar r) = \frac{1}{2}\frac{v(\bar r)}{V_0} = \frac{1}{2}\bar v(\bar r) ; \quad (41)$$

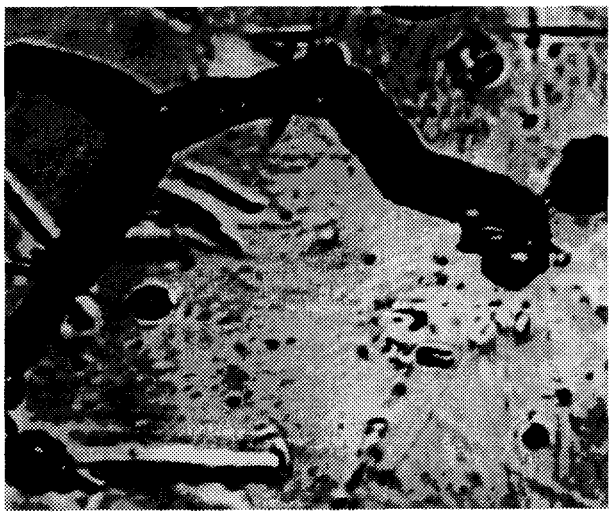
$\bar r = r/r_a$, $\bar z = z/z_a$, and $\bar c = c(x,t)/c_\infty$ are, respectively, the dimensionless values of the radius of the groove, of its depth, and of the concentration $c(x,t)$ of the substance near ($z = 0$) or far from the groove (c_∞).



a



b



c

Figure 8. Model of an etch groove on the GB in thoroughly passivated metals (*a*) and the grain-boundary dissolution of hydrogen-saturated nickel (*b*) and 12X18N9T steel (*c*) polycrystals (× 960).

The boundary conditions are

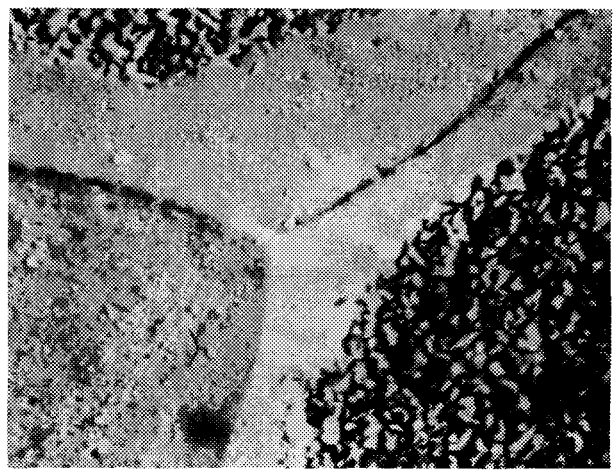
$$\bar{c}\Big|_{\bar{z}=0} = 1, \quad \frac{\partial \bar{c}}{\partial \bar{r}}\Big|_{\bar{r}=0} = 0 \text{ , and } \frac{-\partial \bar{c}}{\partial \bar{r}}\Big|_{\bar{r}=1} = K_D \bar{c} \text{ ,}$$

where $K_D = kr_a/D_A$, and k is a constant.

The solution of the diffusion equation is

$$\bar{c} = \frac{1}{\Gamma(4/3)} \int_{\eta}^{\infty} \exp(-\eta^3) \mathrm{d}n \text{ ,} \tag{42}$$

a



b



Figure 9. Dissolution of iron (*a*) and nickel (*b*) tricrystals (× 12000).

where $\eta = \bar{s}/(9/2\bar{z})^{1/3}$, $\Gamma(4/3) = 0.8934$ is the gamma-function, and $\bar{s} = Pe^{1/3}(1-\bar{r})$. The rate of dissolution in the groove is

$$i_{GB} = \frac{D_A c_B}{0.8934a} \left(\frac{9}{2}\bar{z}\right)^{-1/3} Pe^{1/3} \text{ ,}$$

where a is the lattice constant.

The model proposed by Peschke et al.[37] can be used to describe the dissolution of very pure metals in nonpassivating electrolytes, when $i_{GB} \approx i_{S,\perp}$. The bulk of the grains dissolves at different rates, depending on the crystal orientation of the adjacent single-crystal planes (*hkl*) in contact with the electrolyte (Fig. 9). As a result, some grains dissolve faster than others, and this is the main reason for the formation of a rough surface when a polycrystal is etched.

In a more realistic model the parameter r_a (the radius of the etch groove) varies nonlinearly along the normal z, and in the bulk of the metal $i_a \to 0$. In this case, $i_{GB} > i_{S,\perp}$. The analysis of this model is similar to the analysis of the diffusional permeability of the GB, in which surface diffusion does not play a dominant role.[10] In this model the layer concentration is

$$\bar{c} = \frac{8c_0 r_a}{\lambda} \int_0^{\infty} \operatorname{erfc}(\theta) \operatorname{erfc}\left(\frac{\omega}{2\sqrt{2\theta}}\right) \mathrm{d}\theta \text{ ,} \tag{43}$$

where $c_0 = c'(0,t)$ is the surface concentration, $\lambda = a/\sqrt{Dt}$ is a kinetic parameter, and $D = [(\sqrt{D_1} + \sqrt{D_2})/2]^{-2}$ is the effective bulk diffusion coefficient. As the corrosion process develops according to this model, a very harmful stress concentrator (with sharp notches) is formed on the metal surface and seriously degrades the strength of the metal under mechanical loads.

Experimental studies of the corrosion-induced breakdown of bicrystals began many years ago. The early work of Pfeil [50] showed that an iron bicrystal saturated with hydrogen splits into the two individual single crystals under the influence of applied mechanical stresses. Bicrystals of the *d* metals (V, Nb, Ta) offer convenient samples for the study of intercrystallite dissolution. These can be prepared by electron-beam zone melting with almost any misorientation angle θ. Estimates of the corrosion stability of symmetrical GB have shown [51] that the highest solubility is found in boundaries consisting of the least close-packed (100) and (110) planes of f.c.c. crystals.

The GB in a bicrystal effectively suppress the motion of dislocations, and therefore the dislocation density is higher in a bicrystal than in a single crystal grown under the same conditions. The effectiveness of this suppression depends on the angle θ. The GB with $\theta > 25°$ are less penetrable: on these boundaries, both the dislocation density and the rate of corrosion are enhanced.

When interpreting the changes in the rate of corrosion (K) along the boundary of a niobium crystal, we need to know both θ and the crystallographic orientation of the contacting single-crystal planes (hkl), and also the direction of the rotation angle of the grains ($\bar{n}$), since the parameter K for the given surfaces depends on their crystallographic direction [hkl]. It has been shown [41] that, at a [011]/[0$\bar{1}$1] boundary with $\theta = 16°$, the rate of corrosion and the depth of corrosional degradation (z_{cor}) are highest. The resulting concentration profile is asymmetric, because of the difference between the K values for the different faces. Linear relationships between θ and z_{cor} are observed only for $\theta \leqslant 20°$. Beyond this point, the linearity is perturbed, and at $\theta = 28°$ the plot of z_{cor} against θ develops a minimum apparently associated with a change in the structure of the GB with increase of θ. Whereas at low misorientation angles ($\theta < 20°$) the number of overlapping units decreases monotonically as θ is increased, when $\theta \geqslant 20°$ their number can increase at first and then fall sharply.

The dependence of the rate of corrosion on the reciprocal volume density of overlapping units Σ is nonmonotonic. Extrema in the dependence of K on Σ are found on GB, [13,14] in which the rotation axis is ⟨100⟩ for a GB with $\Sigma = 5$ {210} and $\Sigma = 5$ {310}, and also for a ⟨110⟩ axis for a GB with $\Sigma = 27$ {115} and $\Sigma = 11$ {113}. These data were confirmed experimentally by Miura and coworkers, [51-53] who showed that a copper bicrystal with $\Sigma = 3$ {111} dissolves much more slowly on the GB in 1 M $NaNO_2$ at 300 K than when $\Sigma = 9$ {221} and $\Sigma = 11$ {311}.

It follows from geometric considerations [54] of the structure of the GB that

$$\Sigma = m^2 + n^2(h^2 + k^2 + l^2) ,$$

$$\theta = 2\tan^{-1}\left(\frac{m}{n}\sqrt{h^2 + k^2 + l^2}\right) ,$$

where m and n are integers, and the Miller indices h, k, and l are determined by the vector of the rotation axis of the grains in the bicrystal. In cubic crystals, the following relationship is obeyed between the reciprocal density Σ and the angle θ:

$$\Sigma = \frac{n}{4}\left(1 + \cot\frac{\theta}{2}\right) , \qquad (44)$$

in which a well defined angle θ corresponds [54-56] to each value of Σ and n.

The intercrystallite dissolution (corrosion) (ICC) of various strongly passivating steels has attracted extensive studies. At the potentials of the active–passive transition some stainless steels have dis-solution currents on the grain-boundary bulk approximately 10^4 times greater than materials which are stable towards ICC. The two most commonly used tests for ICC are based on this effect: [57] Strauss's test [boiling the stainless steel samples in a solution of $H_2SO_4 + CuSO_4 + Cu$(powder), $t > 3.6 \times 10^4$ s], keeping the potential at $E = 0.35 \pm 0.03$ V, and Gouy's test (the sample is boiled, in cycles, in 65% HNO_3, $t > 8.6 \times 10^5$ s, and $E = 1.20 \pm 0.05$ V), i.e. the action of strongly oxidising media in the potential region of the transpassive state is simulated). For steels with a well-defined structure and known heat treatment regimes, we can use nondestructive electrochemical potentiostatic and galvanostatic control methods, based on etching in solutions containing chloride ions. One of the latest modifications of these methods [3] consists in analysing the anodic polarisation curves obtained by the potentiokinetic method ($V_E = 3.3 \times 10^{-3}$ V s^{-1}) in a solution of 10% H_2SO_4 + 0.0025 g l^{-1} KCNS. The curves are plotted from $E = 0.75$ V after a preliminary cathodic polarisation (−0.35 V, $t = 60$ s) and an anodic etch in the same solution (0 V, $t = 180$ s). If an anodic loop is not formed on the polarisation curve, the steel is not undergoing ICC. The liability to ICC is assessed [58] from the current in the active state, or from the ratio of the quantities of electricity passing through the electrode when the polarisation curve is plotted in the forward and in the reverse direction. If this ratio is >1, the steel is liable to ICC.

The dissolution currents on the grain-boundary volumes of austenitic stainless steels depend on the segregation of the impurities B, C, N, O, Si, P, and S. Allowance is needed not only for the chemical aspects of the interaction of these impurities with the atoms of the matrix but also for the elastic distortions produced on the GB by the segregation of the impurities. The harmful effect of these impurities on the ICC can be overcome by introducing antisegregants into the metal: additives which chemically bind the impurity by forming an inactive compound. This technical process arose from studies of the effect of hydride-forming impurities on the corrosion and on the physico-mechanical characteristics of hydrogenated polycrystals. When a metal is saturated with hydrogen, the impurities concentrated on

Table 1. The values of Σ and θ for the (100) and (111) planes of the grain boundaries (twisting of the cubic lattice and the misorientation angles for $\Sigma = 3$ and the possible values of n in the X-ray diffraction model).

(100)		(111)		$\Sigma = 3$	
Σ	θ/deg	Σ	θ/deg	Σ	θ/deg
5	36.87	3	60.00	1	33.56
13	22.62	7	38.21	2	48.19
17	28.07	13	27.80	3	60.00
25	16.26	19	46.83	4	70.53
29	43.60	31	17.90	5	80.41
37	18.92	37	50.57	6	90.00
41	12.68	43	15.18	7	99.59
53	31.89	49	43.57	8	109.47
61	10.39	61	52.66	9	120.00
65	14.25	67	24.43	10	131.81
65	30.51			11	146.44
73	41.11				

the GB can form hydride phases, which grow from well defined generation centres. The growth kinetics of these phases are controlled by surface diffusion, by diffusion along the GB, or by the dislocation creep of the metal. In the first case, the rate of change of the radius r of a bubble of the hydride phase (for example, methane) is given by the equation[63]

$$\left(\frac{dr}{dt}\right)_{Sd} = \frac{27}{64}\left(\frac{B}{\Omega_b^3 \Delta^3}\right)[(1+Q\varepsilon\Delta)^{1/2}-1]\left[\frac{1}{Q^3(1-d^2)^3}\right], \quad (45)$$

where $B = D_S\delta_S\Omega\gamma_S/k_BT$ [D_S and D_{GB} are the coefficients of surface and of grain-boundary hydrogen diffusion, $D_S = D_{0,S}\exp(-Q_S/RT)$, $\delta_S = \Omega^{1/3}$, Ω is the atomic volume, γ_S is the surface energy]; Ω_b is the half-volume of the bubble, $\Delta = D_S\delta_S/D_b\delta_{GB}$ [$D_b = D_{0,b}\exp(-Q_b/RT)$, δ_{GB} is the thickness of the GB],

$$Q = \frac{3d}{(1-d^2)^3}\left[\ln\frac{1}{d} - \frac{(3-d^2)(1-d^2)}{4}\right],$$

$$\varepsilon = \frac{2p_{CH_4}\Omega_b}{\gamma_S}, \qquad d = \frac{r}{\Omega_b}.$$

If grain-boundary diffusion is the rate-controlling step of the process, the growth rate of the gas bubble on the GB is

$$\left(\frac{dr}{dt}\right)_{GB} = \frac{3\Omega D_b\delta_{GB}}{d(1-d^2)^2 Q k_B T\Omega_b^2}\left[p_{CH_4} - \frac{\gamma_s(1-d^2)}{d\Omega_b}\right]. \quad (46)$$

Lastly, in the case of dislocation creep, when the growth of the bubble depends on the hydrogen–dislocation interaction and on the quantity of hydrogen transferred with the moving dislocations, the kinetics are described by the expression[64]

$$\left(\frac{dr}{dt}\right)_{dc} = \sqrt{3}\varepsilon_{cr}^0 G_c(d), \quad (47)$$

where

$$\varepsilon_{cr}^0 = \frac{AD_L b}{V_0 k_B T G_c^{N-1}}\left[p_{CH_4} - \left(\frac{2\gamma_S}{r}\right)^N\right],$$

$$G_c = \left(\frac{3}{2}N\right)^N \frac{\Omega_b d}{(1-d^{3/N})^N}.$$

Here A is a constant dependent on the material [see formula (18)], D_L is the coefficient of lattice (volume) diffusion of hydrogen, V_0 is the rate of dislocation creep, and N is the extent of creep.

Under the conditions $r^2 \ll n^{-1} \ll D_L t$, the radius of spherical formations deposited along the GB can be determined by the formula

$$r(z,t) = r(0,t)\left[1 + \left(\frac{2\pi n D_L}{15\delta_b D_{GB}}\right)^{1/2} z r^{1/2}(0,t)\right]^{-2}, \quad (48)$$

where n is the density of the generation centres of the new phase, and δ_b is the diameter of the bubble.

Point defects interact strongly with the GB, and therefore very pure bicrystals must be used in studies of the effect of small, mobile impurities (for example, the hydrogen isotopes). The segregation on the GB of impurities of the *s* and *sp* elements with atoms larger than those of the matrix strongly perturbs the GB structure and alters its hydrogen adsorption capacity.[66] The effective diffusion coefficient of hydrogen $D_{H,ef}$ in the grain-boundary volumes of the transition metals is almost two orders of magnitude greater than through the grain itself. The parameter $D_{H,ef}$ is strongly dependent on the angle θ. The most important experiments were carried out on Pd electrodes, but work on the 3*d* metals has also been reported. Thus, in a calculation of the diffusion coefficients in a bicrystal of very pure (99.999%) nickel with symmetrical boundaries having slopes of 39° ($\Sigma = 9$) and 129° ($\Sigma = 11$), it was found that $D_{D,ef}$ is 4.6×10^{-13} cm s^{-1} in the former case and 8–17 times greater in the latter.

The concentration of hydrogen in the grain boundary volumes induces a phase transformation and the formation of hydrides on the GB; the quantity $D_{D,ef}$ for the hydrogen-saturated nickel polycrystal is $\sim 3 \times 10^{-16}$ m^2 s^{-1}. The specific volume (density) of the hydride is usually different from that of the hydrogen-saturated matrix (the body of the grain). The dilatation effect arising under these conditions induces active processes involving the multiplication of dislocations in the crystallites. The hydrogen transferred together with the moving dislocations promotes further saturation of the GB by hydrogen.[68]

The cluster modelling of the GB on the basis of structural elements with octahedral and tetrahedral pores filled with the impurity atoms has shown[69] that the grain-boundary cohesion increases after the introduction of boron into nickel; it decreases if sulfur is concentrated on the GB. The first cluster calculations have been performed by Hashimoto's group for GB with $\Sigma = 5$ in iron containing phosphorus segregations.[70] Depending on the ratio of the dimensions of the pores and the impurity atoms, directed deformations on the GB can occur for steric reasons, inducing local phase transitions. The interatomic covalent bonds between the atoms of the matrix and the impurities are then strengthened, but the M–M bonds are weakened, the degree of weakening depending on θ and Σ. Subsequently, the influence of the impurities on the properties of many adsorbed surface phases was estimated and phase diagrams for the GB were constructed.[71]

Surface-active impurities, namely P, As, Sb, S, Se, Te, and Sn, greatly reduce the grain-boundary cohesion strength in iron and stainless steels, Si slightly reduces the cohesion, while Ni, C, and B increase it. The addition of N, C, and B slightly alters the segregation of the impurities of the first group on the GB. When the M–electrolyte interface is acted upon by electrolytes, there is a change in the pattern of the mutual influence of the impurities. The affinity of the impurity element for oxygen begins to play a dominant role. Technological additions of boron initiate ICC most vigorously in highly oxidising media — the effect of 0.001% B (X2ON20 steel) is analogous to the effect of ~0.1% P or ~1% Si.[72] The joint introduction of the C and P impurities, of C, and of doping amounts of Si results in the synergism of their activity associated with the localisation of chromium on the grain-boundary volumes in steel. The synergism can be accounted for by the grain-boundary segregation of C and P, inducing the depassivation of the GB as a result of the formation of less ordered oxide layers. An increase in the C content in steel ($0.1 < c_C < 0.3\%$) lowers the concentration of chromium on the grain boundaries as a result of the formation of the carbide $(Cr, Fe)_{22}C_6$ and hence impairs the passivation characteristics locally. However, the supersaturation of the near-surface layer of stainless steel (12X18N9T) with carbon ($c_C > 0.3\%$) increases its tendency towards ICC,[73] since the differences between structures of the oxide layers on the GB and on the body of the grain vanish.

Chromium actually diminishes the rate of dissolution of stainless steel in the passive range of potentials; the introduction of Ni, Mo, and N has a weak effect on the passivation of steel, but suppresses its dissolution in the active region. In the active dissolution of stainless steel, its near-surface layer is enriched in chromium and molybdenum, so that the formation of Cr–Mo–Ni intermetallic compounds as well as nitrides becomes possible. For equal amounts of carbon in austenitic stainless steels of different brands, the tendency towards intercrystallite corrosion is smaller for steels with a higher molybdenum concentration.[74] The joint action of chromium and other doping components (Ti, Ni, Mo, N) increases the zone corresponding to their influence on ICC. The width of the etch channels in ICC on GB is significantly greater (by a factor of 10–100) than the width of the boundary zones depleted in chromium. The width of the depleted zones in austenitic seals of the 304L and 316L types is not more than 1–2 μm. Consequently, in estimating the ICC, it is

necessary to take into account the influence and distribution of other impurities, in particular nitrogen.

Nitrogen, localised on structural defects, suppresses the selective dissolution of steel, which lowers the rate of corrosion. The sharp decrease in the solubility of transition metals after saturation with nitrogen is a well known phenomenon used in engineering. However, the concentration of nitrogen in steel must be maintained at a level $c_N \leqslant 0.13\%-0.15\%$ or $0.4\%-0.5\%$ (superaustenitic steels). Such a steel is resistant to the action of oxidation-reduction media and does not undergo ICC and slit corrosion in halide-containing solutions.[75] For $0.15\%-0.18\% < c_N < 0.4\%$, nitrides ($Cr_2N$) are formed vigorously and the rate of corrosion on the GB increases.[74]

The crystallographic stability is lost more readily on the GB, the overvoltage η being appreciably smaller than on the body of the grain. Correct crystallographic solutions of problems concerning the grain-boundary dissolution have been published by the groups of Froment and coworkers[13,14] and Gleiter.[76,77] Geometrical calculations are performed starting with the postulate that the rates of dissolution of neighbouring grains are different, so that the misorientation angles relative to the normal to the GB are also different. This makes it possible to calculate the changes in the surface tension $d\gamma$ by Eqn (15). The grain-boundary volume itself is not taken into account in such models; it is also disregarded in the CBL, GDL, and FOL models.

The grain-boundary dissolution process depends in many respects on the misorientation angle θ. By means of the texturing treatment of rolled sheet steel, it is possible to achieve changes in the rate of corrosion by several orders of magnitude and also to avoid the need for the use of corrosion inhibitors. There are definite critical angles θ_{cr} below which the GB have a low energy.[78] With increase in θ, the depth of the ICC increases and the stability of the GB falls. The decrease in the stability of the GB may be accompanied by the appearance on the bottom of the etch groove of a crack spreading into the bulk of the metal. The development of the crack depends subsequently on the topology and density of the dislocations in the local volumes of the metal. In the vicinity of a GB, there is an extensive dislocation structure with an increased content of mobile impurities. The dissolution process is undoubtedly associated with grain-boundary segregations, phase formation on the internal interfaces on heat treatment, ageing, and saturation with hydrogen.

In the estimation of the degree of corrosion on an interface by standard methods, the overall dissolution current i_Σ is regarded as the sum of the dissolution currents in the defects (i_D) (vacancies, dislocations, grain boundaries) and on the undamaged part of the surface (i_S). An exact quantitative separation of these currents is not always possible. For specimens, where either GB or only the material of the bulk of the grain appear on the working surface, it is possible to employ a novel method proposed by Khaldeev et al.[79] With the aid of this method, the influence of grain-boundary volumes on the electrochemical characteristics of the specimens was estimated experimentally and a study was made[79] of the influence of the vacuum heat treatment (673, 1073, and 1273 K, $t = 5 \times 10^5$ s) of M1 (99.90%) and M00 (99.95%) copper on the physical properties and corrosion in 0.5 M H_2SO_4.

The electrochemical characteristics of specimens annealed at a high temperature (973 and 1273 K for M00 and 1273 K for M1) change abruptly during anodic dissolution (Fig. 10). Thus, in the course of the continuous cyclic recording of polarisation curves for the same M1 specimen, one type *3'* curve is recorded after virtually only one type *3* curve, whilst for M00 copper annealed at 973 and 1273 K a type *6'* curve is recorded after 4–5 type *6* curves.

This can be accounted for as follows. High-temperature annealing leads to the growth of the grain (Fig. 10, curves *1* and *2*) and the formation of the so called bamboo structure, where GB cuts across the cross-section of the specimen in definite steps. The attainment of such boundaries in anodic dissolution leads to the appearance of anomalous $E-i$ curves (curves *3'*, *5'*, and *6'*), which has been confirmed by a parallel microscopic study. The

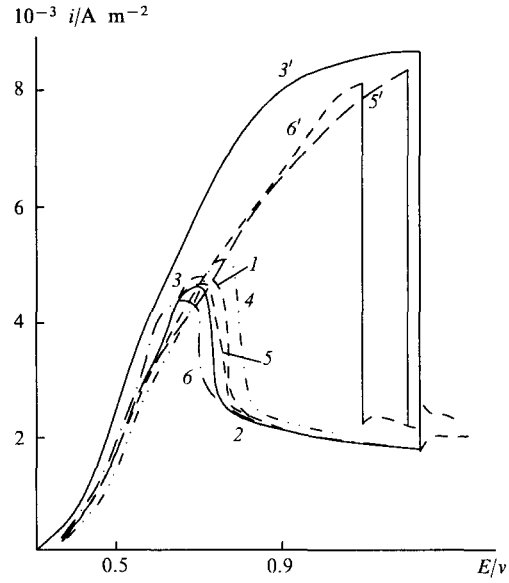


Figure 10. Anodic potentiodynamic ($V_E = 8 \times 10^{-4}$ V s^{-1}) curves for M1 (curves *1–3* and *3'*) and M00 (curves *4–6*, *5'* and *6'*) copper in 0.5 M H_2SO_4. Annealing temperature (K): (*1*) and (*4*) 673; (*2*), (*5*) and (*5'*) 973; (*3*), (*3'*), (*6*) and (*6'*) 1273.

formation of such a structure depends on the purity of the metal; in purer copper (M00), the grains are larger. At $T = 1273$ K, the grain diameter is $d_{M00} = 0.5-1.0$ mm, whereas $d_{M1} = 0.1$ mm, the value of d along the axis of the specimen being several times greater. Thus the highly pure M00 copper annealed at 1273 K contained a bicrystal in its cross-section as well as in the case where a layer with short GB was dissolved (a layer 0.03–0.05 mm thick dissolved during the recording of one curve); an almost twofold increase in i_{max} and E_{max} was observed [from $(4.5-4.6) \times 10^3$ to $(8.5-8.8) \times 10^3$ A m^{-2} and from 0.65–0.70 to 1.10–1.30 V respectively].

The purity of the metal influences significantly the mobility of the boundaries during annealing; as a rule, the impurities are concentrated in the vicinity of the GB. The accumulation of impurities on the GB may be regarded as a phase transition involving a change in the type of bond — from metallic in the bulk phase to predominantly covalent on the GB. This makes it possible to explain the differences in the behaviour of M1 and M00 copper. The anomalous dissolution is apparently not associated with changes in the nonequilibrium defects within the grain. With increase in the annealing temperature above 973 K, the relative resistance $K_\rho = \rho_{233}/(\rho_{293}-\rho_{77})$ (here ρ_{293} and ρ_{77} are the specific resistances at 293 and 77 K respectively), which makes it possible to estimate the degree of defectiveness of the GB of the grains, increases rapidly (Fig. 11, curves *3* and *4*). This indicates an increase in the degree of defectiveness in the region of the grain boundaries. Measurements of the internal friction Q^{-1} also indicate that a more ideal structure is created within the grain (Fig. 11, curves *5* and *6*). The nature of the variation of Q^{-1} shows that the movement of the dislocations within the grain is responsible for the increase in the internal friction: with increase in the size of the crystallites, there is an increase in the length of the dislocation segments between the points of strong attachment and the localisation of the impurities in the region of the GB promotes a smaller degree of blocking of the dislocations by the impurity atoms (Fe, Zn, Sb, Bi, P). The changes in i_{max} and E_{max} are not associated with the morphology of the intragrain volumes, since, according to the results of electron microscope analysis, there are no appreciable differences in surface rugosities for the specimens (Fig. 10, curves *1–6*). However, if the dissolution in the active range of potentials takes place on the GB for copper which has

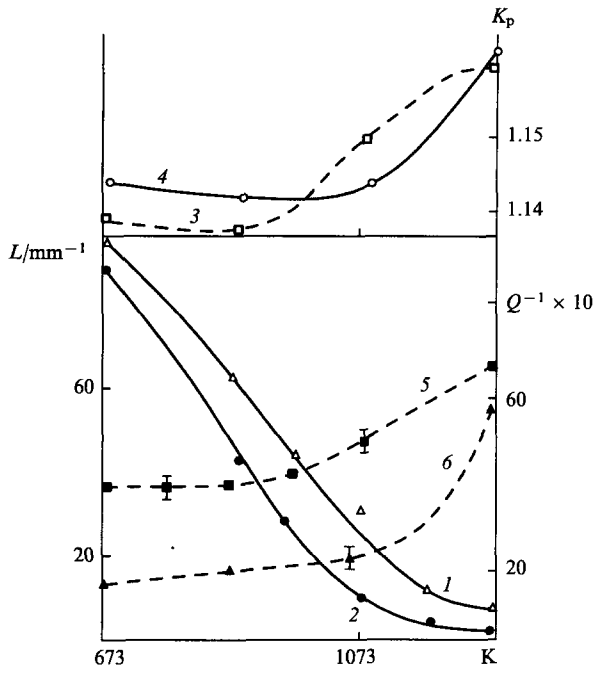


Figure 11. Dependence of the length of the grain boundaries (curves *1* and *2*), the relative electrical resistance (curves *3* and *4*), and the internal friction (Q) at a frequency of 1 Hz (curves *5* and *6*) on the annealing temperature for M1 (curves *1–3*) and M00 (curves *4–6*) copper.

been subjected to high-temperature annealing, the formation of etch channels is noted. Thus a decrease in the length of the GB and an increase in the concentration of defects and impurities in their vicinity may induce an appreciable anomalous change in the dissolution currents and passivation potentials.

Erb et al.[76] reached a similar conclusion. The method used in their experiment reduces to the following. In order to achieve the separate quantitative estimation of the rates of corrosion on the GB and on the bulk of the grain, two highly pure copper crystals (99.999%) and a Cu–Bi copper alloy (6×10^{-3}–7×10^{-2} at.% Bi) were sintered, after which only the GB (at $T = 263$ K, $t = 5.4 \times 10^5$ s) was subjected to corrosion in aqueous 12% HCl solution to which 1 g litre^{-1} of $FeCl_3.6H_2O$ had been added. The width of the etch groove formed is ~20–45 μm. The development of the ICC is associated with the increase in the local anode current i_a, caused by the accumulation of the bismuth impurities, and not with the increase in γ_{SL} (the free energy of the region of the metal lattice near the GB).

The analysis of the behaviour of triple grain contacts is important in the description of the stable networks of grain-boundaries on the surface of the crystal. On the basis of the modified Mullins model,[47] results have been obtained[70] according to which the region of the triple contact increases on dissolution and does not undergo a change in shape, the latter being determined solely by the free energy of the boundaries. The crater region of the contact is larger than the etch groove and its size increases with decrease in the angle between the boundaries converging at the point of contact. The corrosion-activated triple contact of the GB (and the GB themselves in textured materials) may become a dangerous concentrator of the disruption. Following the application of a load in excess of the ultimate strength and acidification of the medium in the corrosion pit, the crack increases catastrophically.[81] The rate of the abrupt growth of such a crack into the bulk of the material obeys a relation[81] analogous to the Kolmogorov–Johnson–Mell–Avraami equation:

$$V_c = \left[0.5m + \frac{\Delta a_p}{V_\delta}\left(1 - \exp\frac{-V_{\delta,S}}{t_p V_\delta}\right)\right] V_\delta \ , \qquad (49)$$

where m is the characteristic of the profile of the sloping side of the groove [Eqn (34)], Δa_p the sum of the changes in the internal conditions (constants of the material) and external conditions (the potential E, the rate of deformation V_d, and the composition and concentration c of the solution), and V_δ and $V_{\delta,S}$ are respectively the overall rate of expansion of the plastic failure zone (abrupt growth of the crack) and the corresponding rate in a single act. The abrupt growth is effected as a result of the formation of steps, which is accompanied by an increase in the rate of corrosion i_{cor}. The crack is initiated within narrower ranges of E and V_d than its propagation and depends greatly on the angle θ and the reciprocal of the density of the coincidence blocks Σ. The values of θ and Σ for which the M–M bonds are anomalously weakened are characteristic also of intense ICC.

VI. Dissolution of heterophase polycrystalline metals

The influence of bulky defects (microinclusions) on the dissolution of a metal must be considered in terms of a continuous approximation. The intragrain heterogeneity may be caused not only by mesolevel defects (single dislocations, low-angle boundaries of dislocation origin, and coherent binary layers), but also by rigid inclusions inducing both elastic and plastic deformation of the material of the grain. As a rule, the rates of dissolution of the inclusion and the matrix are different, while the stresses generated by the inclusions in the matrix are capable of altering significantly the rate of corrosion of the metal.

The role of nonmetallic inclusions in the corrosion process is complex: depending on their type and geometry, the rate of dissolution of the metal may both increase and diminish. Clearly i_{cor}, which depends on the sum of the internal factors (impurity composition, structure, and deformation state of the metal) and external factors (anionic composition and electrolyte parameters), may vary within wide limits, the greatest changes being observed in materials which dissolve under more nonequilibrium conditions (corrosion under stress, corrosion in slits and gaps, corrosion under the conditions of nonstationary movements of the electrolyte, corrosion in the anodic process, etc.).

It is of interest to examine the role of the rigid inclusions in the dissolution of a heterophase polycrystalline metal. This problem is of current interest for composite electrochemical coatings, carbon steels containing cementitic Fe_3C outcrops in ferrite, and also brass, titanium and its alloys (α-phase in a β-matrix), and certain other materials, since it is necessary to take into account the change in the deformation state of the matrix following the development of microinclusions. The rate of dissolution of an elastically deformed metal may increase significantly.

Plastic inclusions. We shall consider a periodic system of linear planar parallel inclusions. Their length is $2l$, their centres are located on the $0x$ axis, and the angles α of their inclination relative to the axis are equal (Fig. 12). In order to find the stresses arising under these conditions, it is necessary to solve the following integral equation:[82]

$$\int_{-l}^{l} [G(\rho, t)K(t - x, \rho^*) + G(\rho, t)L(t - x)]\mathrm{d}t = 0.5\pi i(\rho - \rho^*)F(\rho^*, x), \quad |x| < l \ , \qquad (50)$$

where

$$K(x, \rho^*) = 0.5\pi\rho^* l_d^{-1}\{\exp(i\alpha)\cot[\pi x \exp(i\alpha)]l_d^{-1}\} + \exp[(i\alpha)\cot(-i\alpha)]l_d^{-1} \ ,$$

$$L(x) = 0.5\pi l_d^{-1}\{\cot[\pi x \exp(-i\alpha)]l_d^{-1}\} - \pi x[\exp(-i\alpha)]\mathrm{cosec}^2[\pi x \exp(-i\alpha)]l_d^{-1}[\exp(-i\alpha) - \exp(-3i\alpha)]\cot[\pi x \exp(-i\alpha)]l_d^{-1} \ ,$$

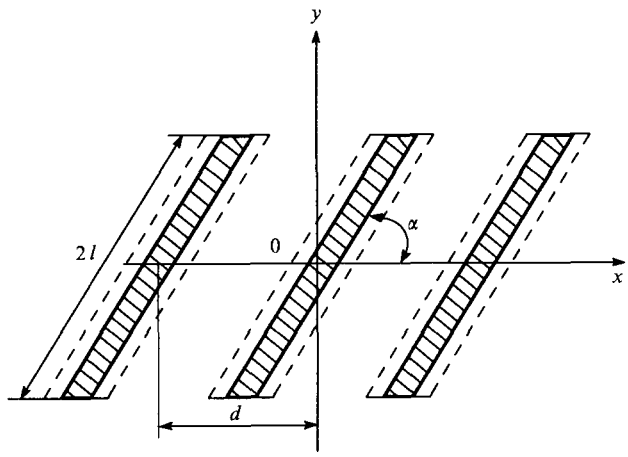


Figure 12. Schematic illustration of the matrix–rigid inclusion system.

$G(\rho,t)$ is a stresses function, $F(\rho^*,x)$ is a known displacement function, and ρ^* assumes the values L and $-l$ for rigid inclusions. The solution of this equation must satisfy the condition

$$\int_{-l}^{l} G(\rho,t)\mathrm{d}t = 0 \ .$$

Having expressed $G(\rho,t)$ in the form

$$G(\rho,t) = U(\rho,t) + \mathrm{i}V(\rho,t) \ ,$$

we obtain

$$\bar{G}(\rho,t) = U(\rho,t) - \mathrm{i}V(\rho,t) \ .$$

Having expanded the functions $\cot\varphi$ and $\mathrm{cosec}^2\varphi$ in a power series and having retained only the first two terms of the expansion (since they make the greatest contribution to the expansion for short distances between the defects), we obtain the following expressions for $K(x,\rho^*)$ and $L(x)$:

$$K(x,\rho^*) = \frac{\rho^*}{x} - \frac{\pi^2\rho^*\cos 2\alpha}{3l_\mathrm{d}^2}x \ ,$$

$$L(x) = \left(-\frac{2\pi^2}{3l_\mathrm{d}^2}\sin 3\alpha \sin\alpha\right)x + i\left(\frac{2\pi^2}{3l_\mathrm{d}^2}\cos 3\alpha \sin\alpha\right)x \ .$$

Having expressed $G(\rho,t)$ and $\bar{G}(\rho,t)$ in the form $G(\rho,t) = a_0 + a_1\rho + a_2 t + \mathrm{i}(b_0 + b_1\rho + b_2 t)$, i.e. containing only the linear terms in the expansions of $G(\rho,t)$ and $\bar{G}(\rho,t)$, we obtain a system of equations for the determination of the coefficients a_2 and b_2:

$$\begin{aligned} &a_2\left[\rho^*\left(2l + x\ln\left|\frac{l-x}{l+x}\right|\right) - \frac{l^3}{3}\frac{\pi\rho^*\cos 2\alpha + 3\pi^2\sin 3\alpha\sin\alpha}{3l_\mathrm{d}^2}\right] \\ &\quad - b_2\frac{2\pi^2}{3l_\mathrm{d}^2}\cos 2\alpha\sin\alpha = 0.5\pi(\rho^* - \rho)B \ , \\ &- a_2\frac{2\pi^2}{3l_\mathrm{d}^2}\cos 3\alpha\sin\alpha \\ &\quad + b_2\left[\rho^*\left(2l + x\ln\left|\frac{l-x}{l+x}\right|\right) - \frac{l^3}{3}\frac{\pi\rho^*\cos 2\alpha}{3l_\mathrm{d}^2}\right. \\ &\quad \left. + \frac{l^3}{3}\frac{3\pi^2\sin 3\alpha\sin\alpha}{3l_\mathrm{d}^2}\right] = 0.5\pi(\rho - \rho^*)A \ . \end{aligned} \tag{51}$$

Here $A(\rho^*,x)$ and $B(\rho^*,x)$ are the real and imaginary components of the function $F(\rho^*,x)$. The coefficients a_0, a_1, b_0, and b_1 do not enter into the expansion in view of the symmetry of the function $G(\rho^*,x)$, because in this case $a_0 + a_1\rho = 0$ and $b_0 + b_1\rho = 0$.

Having solved Eqn (51), we obtain expressions for the coefficients a_2 and b_2:

$$\begin{aligned} a_2 &= \frac{-0.5\pi(\rho - \rho^*)B(\rho^*,x)}{\rho^*\left(2l + x\ln\left|\frac{l-x}{l+x}\right|\right) - \frac{l^3}{3}\frac{\pi\rho^*}{3l_\mathrm{d}^2}} \ , \\ b_2 &= \frac{0.5\pi(\rho - \rho^*)A(\rho^*,x)}{\rho^*\left(2l + x\ln\left|\frac{l-x}{l+x}\right|\right) - \frac{l^3}{3}\frac{\pi\rho^*}{3l_\mathrm{d}^2}} \end{aligned} \tag{52}$$

We shall consider the special case where the displacements are directed along the $0x$ axis. Analysis of the expressions for the coefficients a_2 and b_2 yields the following results: if $\alpha = 0$, then the stresses fall to zero for $l_\mathrm{d}\to 0$ and approach asymptotically a definite value for $l_\mathrm{d}\to\infty$. For a fixed distance l_d, the stresses vary as a function of x—the stresses diminish on moving away from the boundaries of the rigid inclusions. The curve relating the stresses to the distance to the GB has a minimum. We may note that the influence of the thickness of the inclusions on the distribution of the stresses is taken into account by the quantity l_d.

In the case of a uniform distribution of lamellar segregations in the matrix, a uniform stresses field arises within the crystals and the average density of the forces corresponds to the distribution of the surface forces. With increase in the number of inclusions of the second phase in a definite volume of the crystals, the overall surface energy on their interfaces also increases:[83]

$$\Delta\sigma = G_\mathrm{c}g^2\Delta c^2\mathrm{d}A_\mathrm{S}^2 + \frac{\gamma A_\mathrm{S}^3}{l_\mathrm{d}} \ ,$$

where $g = \mathrm{d}a/\mathrm{d}c$ is a derivative characterising the coherence of the transition on the interface, a the lattice parameter of the matrix, $\Delta c \approx \Delta\gamma^{\neq}$ the difference between the concentrations of the species in the phases proportional to the degree of supersaturation, A_S the area of the lamellar inclusions, and γ the surface tension. The minimum in $\Delta\sigma$ is observed for $\gamma = G_\mathrm{c}A_\mathrm{S}^{1/2}$. On formation of noncoincidence dislocations (ND) on the interfaces and also by virtue of the intensification of the diffusion of impurity atoms in the field of the elastic stresses of the species comprising the second phase, the stresses in the heterophase structure relax. The creation under these conditions of a sharp concentration profile of the impurities in the near-surface layer of the lamellar outcrops and the consequent dilatation effect induce an additional influx of impurities into this zone—an autocatalytic growth of inclusions takes place.

The physical picture of the distribution of stresses in the matrix and in the vicinity of the interfaces, obtained in terms of the continuous approximation within the framework of the linear theory of elasticity, is almost equivalent to the representation of the distribution of the dislocations at the interfaces. In the immediate vicinity of the interface, there are zones in which there is a sharp decrease in the level of the stresses and in the concentrations of the elementary deformation carriers. Subsequently they increase sharply. The background values of σ and ρ_d are attained for distances greater than the size of the dislocation (> 1 μm). It is clear from the foregoing that the superfine-grained materials with a grain size $\leqslant 1$ μm have unique physicochemical characteristics and an increased corrosion resistance.

Spherical inclusions. Apart from lamellar inclusions, intragrain heterogeneity is induced by spherical inclusions.

We shall consider the appearance of stresses in the matrix in the vicinity of spherical dispersed particles (DP) without taking

into account the chemical nature of the latter. A continuous theory for the estimation of stresses in the vicinity of single particles of subatomic dimensions has been thoroughly developed and described.[84] The introduction of DP with a volume V and a surface area A_S into the crystals is accompanied by an increase in the volume of a finite crystal by ΔV and the appearance of a stress field. For a uniform distribution of N dispersed particles, the average stress

$$\langle\sigma\rangle = \frac{N}{V}P_d ,$$

and the average deformation

$$\langle\varepsilon\rangle = \frac{N}{V}A_S P_d .$$

(here P_d is the force dipoles tensor characterising the direction of the forces of the effect of DP on the matrix) are inversely proportional to the volume of the DP; for high ratios NA_S/V, the quantity $\langle\varepsilon\rangle$ should increase. The latter is characteristic of DP distributed uniformly in isotropic matrices. However, it can be readily seen that the average stress $\langle\sigma\rangle$ diminishes with decrease in the volume of the DP: the decrease in the level of the stressed state of a heterophase material as well as the creation of a uniform deformation should naturally promote an increase in its corrosion resistance, because the corrosion-induced destruction of metals is associated with the rupture of the M – M bonds. For ultradisperse particles, it is apparently also possible to confine the treatment to the continuous approximation, since the need for the employment of the microscopic lattice theory arises for mesolevel defects with dimensions less than 50 atomic radii (6–8 nm) — for coagulations of vacancies, clusters of extraneous atoms, dislocations, and disclinations.

We shall consider an assembly of DP in an isotropic matrix in which both the distance between the DP and the dimensions of the DP themselves vary. Such a situation is characteristic of real heterophase materials. The stresses near a single point source act radially and are proportional to x^{-1}, where x is the distance from the DP. If one considers the DP as a point source of stresses with the coordinates (0,0), then the stress at this point (Fig. 13) can be expressed by the relation

$$\sigma_{xy} = \frac{A}{\sqrt{(x-x_0)^2 + (y-y_0)^2}} ,$$

where A is a constant which depends on the material of the matrix. For several sources with coordinates (x_n, y_n), the superposition principle operates and the overall stress σ_Σ can be expressed in the form

$$\sigma_\Sigma = A\sum_{i=1}^{n}\frac{1}{\sqrt{(x-x_i)^2 + (y-y_y)^2}} . \qquad (53)$$

In calculating the sums in Eqn (53), we proceed as follows. Since the DP with the coordinates (0,0) is influenced most by the nearest particles, one can assume that the latter are distributed on a circumference with a radius R (Fig. 13) or on a circular sinusoid.

The stresses in the matrix $(\sigma_{x,y})$ are then formulated as follows:

$$\sigma_{x,y} = A\int_0^{2\pi}\frac{dA_S}{\sqrt{(x-\xi)^2 + (y-\eta)^2}} . \qquad (54)$$

In the parametric form, we have

$$\xi = R\cos t, \quad \eta = R\sin t.$$

Hence $dA_S = Rdt$. Having substituted the last expressions in Eqn (54), we obtain

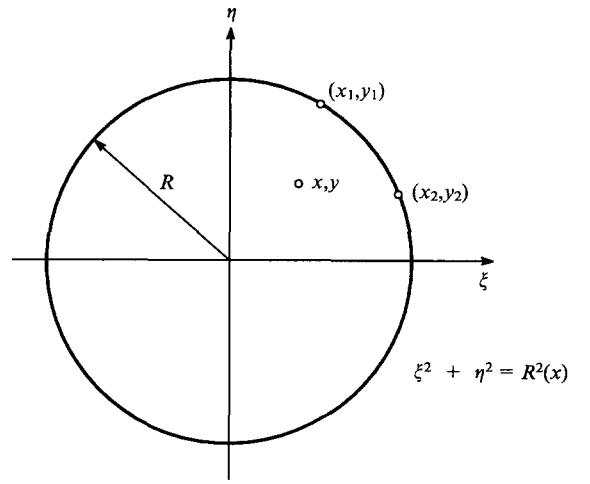


Figure 13. Model illustrating the disposition of disperse particles in a matrix.

$$\sigma_{x,y} = A\int_0^{2\pi}\frac{Rdt}{(x - R\cos t)^2 - (y - R\sin t)^2} . \qquad (55)$$

Since the disposition of the coordinate system (Fig. 13) makes it possible to regard the parameter of the point (x, y), at which the stresses are estimated, as fairly small, the integrand function in Eqn (55) can be expanded in series in x and y:

$$f(x,y) = f(0,0) + \frac{\partial f}{\partial x}(0,0)x + \frac{\partial f}{\partial y}(0,0)y + \frac{\partial^2 f}{\partial x^2}x^2 + 2\frac{\partial^2 f}{\partial x\partial y}xy + \frac{\partial^2 f}{\partial y^2}y^2 + O\left[\left(\sqrt{x^2+y^2}\right)^3\right] . \qquad (56)$$

Having formulated the derivatives for the terms of the integrand function $f(x, y)$, having substituted them in Eqn (56), and having integrated the latter for the stress $\sigma_{x,y}$, we obtain

$$\sigma_{x,y} = 2\pi A + \frac{4\pi A}{R^2}(x^2 + y^2) . \qquad (57)$$

We shall now analyse Eqn (57) taking into account the fact that R is a fixed quantity. For $0 < x < R$, $0 < y < R$, we have $\sigma_{x,y} \to 2\pi A$ if $x \to 0$ and $\sigma_{x,y} \to 10\pi A$ if $x \to R$.

Thus the stresses increase by a factor of 5 with increase in the distance from the DP and reach maximum values in the vicinity of $x = R$.

For spherical ultradisperse particles, the stresses can vary in accordance with a less steep law, in proportion to x^{-2} and not x^{-1}. In this case, the transformation of an equation of type (54) leads to the expression

$$\sigma_{x,y} = \frac{AR}{\sqrt{(x^2 - R^2) + 2y^2x^2}}\left(\frac{\pi}{2} + \arctan\frac{Ry}{(x^2 - R^2) + 2y^2x^2}\right), \qquad (58)$$

the analysis of which shows that the stress on a sphere is significantly smaller. We have

$$\sigma_{x,y} = \frac{\pi}{2}A$$

for $x = 0$ and $y = 0$, and

$$\sigma_{x,y} = \frac{3\pi A}{4R^3} .$$

for $x = R$ and $y = R$.

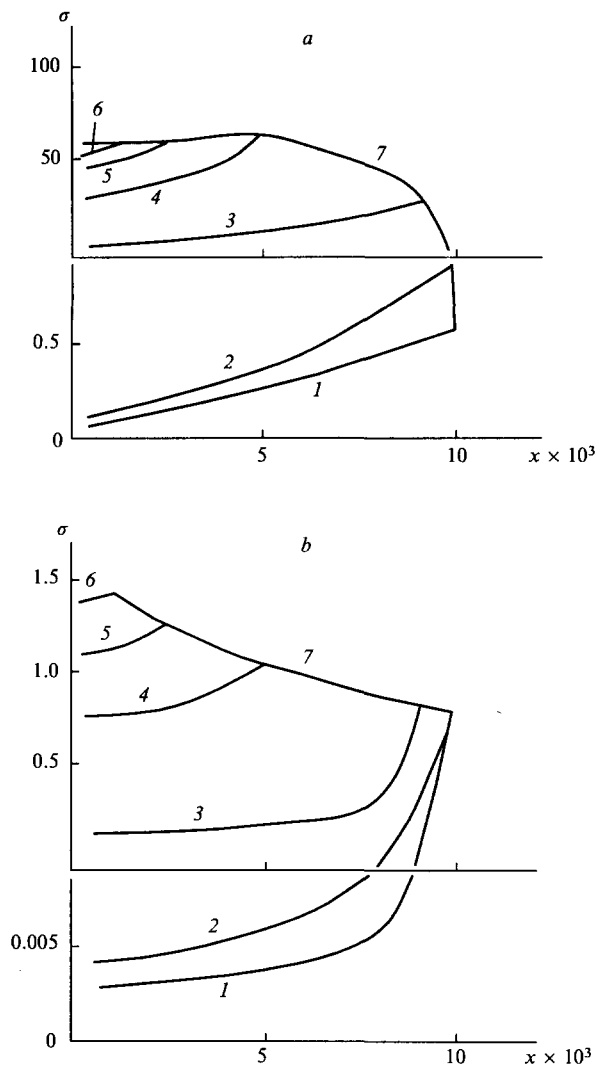


Figure 14. Dependence of the stresses in a matrix on the size of DP and the distance between them. Attenuation of the stresses in accordance with the x^{-1} (*a*) and x^{-2} (*b*) laws: r (nm): (*1*) 20; (*2*) 30; (*3*) 10^3; (*4*) 5×10^3; (*5*) 7.5×10^3; (*6*) 9×10^3; (*7*) stress level on a sphere with a radius $R = 10^4$ nm.

Numerical study of Eqns (56) and (57) for reasonable ratios of the DP radius and the quantity $R = 10^4$ nm (comparable to the grain size usually employed in metal technology) shows that, when the stresses are attenuated in accordance with the x^{-1} law (Fig. 14*a*), the quantity σ on the sphere where the surrounding DP are located is large. With decrease in the size of the DP, the stresses rapidly diminish—the greatest strengthening of the matrix is obtained for $x = 0.5R$ (Fig. 14*a*, curve *7*). When the stresses are attenuated in accordance with the x^{-2} law (Fig. 14*b*), the stresses level in the matrix is 2 orders of magnitude smaller than in the former case, but σ increases markedly in the vicinity of the DP. Under these conditions, the growth of stresses depends significantly on the size of the DP: the smaller the radius of the particles, the sharper the deformation profile (Fig. 14*b*, curves *1–3*). However, in a matrix uniformly saturated by particles the stresses change only slightly (Fig. 14*b*, curve *7*).

Thus the overall level of stresses in the matrix increases with decrease in the size of the DP and the stresses are localised in the vicinity of the DP.

The stresses near the DP relax, forming long noncoincident dislocations (ND) in the matrix. By virtue of this process, the density of dislocations ρ_d increases at the DP–matrix interface and microtwinned formations are produced [the process is usually observed experimentally in the study of thin foils by transmission electron microscopy (TEM)]. The continuous assessment of the stressed state in the vicinity of the DP–matrix interface does not conflict with the calculated model and the experiment on the distribution of dislocations in the vicinity of the grain boundary described above. The presence of an extremum in the stresses in an isotropic matrix promotes the appearance near the interface of zones with a reduced density of defects.

The equilibrium concentration of impurities in the matrix near a spherical particle with a radius r corresponds to the Gibbs–Thomson equation. We formulate this equation in the form

$$c_r(x,t) = c_\infty \exp\frac{2\gamma_{SL}\Omega}{rRT} ,$$

where c_∞ is the concentration of impurities on the inclusion–matrix interface in the case of a planar surface when $r \to \infty$ and $K_M = 0$. Analysis by Lifshits and Slezov[85] showed that, for a certain degree of supersaturation $\Delta\gamma^{\neq} = c - c_\infty = \text{const}$, the quantity

$$r_{cr} = -\frac{2\gamma_{SL}}{\Delta G_V} ,$$

corresponds to the equilibrium between a particle and the impurities near it. Here ΔG_V is the change in free energy in the crystal–liquid transition. The particle grows if $r > r_{cr}$ and is degraded if $r < r_{cr}$. The annihilation of small particles occurs as a result of consecutive pair interactions. Two particles with masses m and n form a new particle with a mass $m - n = k$: for long times t, the concentration of such particles is[86]

$$A_k(t) \sim \frac{A}{t(\ln t)^{k-1}} ,$$

where

$$A_k = \frac{(N-1)!}{(N-k)!} , \qquad k = 1, 2, \ldots, N-1;$$

N is the mass of a particle (cluster) having a finite volume.

The noncoincident dislocations, fixed on the DP, serve as pathways for the diffusional migration of impurities from particles having a low radius and undergoing degradation to larger particles. We shall analyse the growth of such DP in the matrix. For a uniform distribution of the particles (as above, the volume of a matrix having a radius R is considered), the particle is acted upon by a force $F = G_c/r$, the overall vector of which may be random.

If the distribution function for particles in the bulk of the matrix, the volume of which is limited by a radius R, is

$$f_0(R) = \frac{3}{r^3}R^2 ,$$

the overall distribution function can be formulated as follows:

$$g(x,y)\mathrm{d}x\,\mathrm{d}R = g_1(\varphi,R)\mathrm{d}\varphi\,\mathrm{d}R = \frac{3}{r^3}R^2\mathrm{d}R\frac{1}{2}\sin\varphi\,\mathrm{d}\varphi \qquad (59)$$

$$= \frac{3R^3}{2r^3G_c}\mathrm{d}R\,\mathrm{d}x ,$$

where φ is the angle between the specified direction and the direction of the force acting on the particle.

Having integrated Eqn (59) with respect to all R, we obtain the expression

$$f(x) = \frac{3}{2r^3G_c}\int_0^r R^3\mathrm{d}R = \frac{3}{8}\frac{r}{G} , \qquad (60)$$

which is valid for $|x| < G_c/r$. If $|x| > G_c/r$, then

$$f(x) = \frac{3}{2rG_c}\int_0^{G_c/|x|} R^3 dR = \frac{3}{8}\frac{G_c^3}{r^3|x|^4}. \quad (61)$$

It is possible to determine experimentally the distribution of stresses in the vicinity of a charged particle, i.e. the characteristics of such a stress can be estimated before the corrosion test. For example, the average expected stress MF is given by

$$MF = \int_0^\infty xf(x)dx$$

$$= \int_0^{G_c/r} x\frac{3}{8}\frac{r}{G_c}x\,dx + \int_{G/r}^\infty \frac{3}{8}\frac{G_c^3}{r^3}x^{-3}dx = \frac{3}{8}\frac{G_c}{r},$$

and the average scatter DF around this value is

$$DF = \int_0^\infty (x - MF)f(x)dx = \frac{7}{64}\frac{G_c}{r^2}, \quad (63)$$

i.e., for a particular metal, it is found that the smaller the size of the DP the higher the stresses level on the interface. In terms of mathematical statistics, the probability that the specified stress is exceeded is given by

$$P(\beta \leqslant x < +\infty) = \int_\beta^\infty f(x)dx;$$

β has two extreme values: if the concentration of particles is small so that $\beta < G_c/r$, we have $P = 3\beta/16$; if a volume with a radius R is overfilled with particles for $\beta \geqslant G_c/r$, we have $P = G_c^3/8r^3\beta^3$.

Thus, when the quantitative relation between the stresses level σ and the rate of corrosion i_{cor} is known, it is possible to determine the probability that the chemical resistance of the metal will change.

The quantity $\sigma_{x,y}$ was estimated above relative to a particle within the sphere on which the surrounding DP are located. The overall stresses arise as a result of the superposition of the $\sigma_{x,y}$ due to the assembly of DP, whereupon the extremum values of $\sigma_{x,y}$ within the sphere correspond to $x = 0.5R$ when the stresses are attenuated in accordance with both the x^{-1} and x^{-2} laws. It is noteworthy that the electrical characteristics of a surface with periodic inhomogeneities in the near-surface layer of the metal have an extremum at $x = 0.5r$.

Thus analysis shows that within the sphere there is a region with an extremum stresses level. Heterophase materials in which the ratio of the dimensions of the grain and the DP satisfies the condition $x = 0.5R$ exhibit the lowest corrosion resistance. Such situations may arise when two-phase alloys or ferrite-perlitic steels are employed in corrosive media and also for the local formation of hydrides in a matrix where particles of a second phase grow in the course of the hydrogen saturation process and there is a sudden increase in the rate of corrosion.

The relaxation of stresses in the vicinity of the DP takes place also as a result of the dislocation migration of impurities, i.e. as a result of local changes in chemical composition. The dislocation migration depends on the mobility of the dislocations V, which is related, in its turn, to their density by the simple expression

$$V = \frac{\dot{\varepsilon}}{\rho_d b}, \quad (64)$$

where $\dot{\varepsilon}$ is the rate of deformation of the crystal. It follows from Eqn (64) that an increase in ρ_d (for example, from 10^4 to 5×10^{18} m^{-2}) should lower significantly (by a factor of 10^5) the mobility for $\dot{\varepsilon}$ = const. In the case of a hydrogen-saturated metal, $\dot{\varepsilon}$ should lie in the pre-Cottrell region, i.e. V should not exceed V_{cr} ($V_{cr} \leqslant 4D_D r_d^{-1}$, and r_d is the radius of the Cottrell atmosphere of the impurity atoms on a dislocation tube), whereupon dislocations are abstracted from the atmospheres of the impurity atoms. Favourable conditions for the relaxation of stresses and the redistribution of impurities arise at elevated temperatures and for low rates of deformation. For iron alloys, this corresponds to isothermal treatments at T = 400 K and t > 6 ks.

A nonuniform distribution of the DP in the matrix and hence the alternation of zones with different stressed states increases the risk of a sudden disintegration for high degrees of localisation of the corrosion process.

VII. Conclusion

In the physical chemistry of interfacial processes, a steady interest in the study of the influence of the structure of the interfaces on charge and material transfer processes has been manifested recently. The anomalies in the chemical reactivity of grain boundaries compared with the surfaces of crystals having structural defects with a definite structural hierarchy are due to their unusual structure. These anomalies can be used in electrocatalysis, in the electrosynthesis of organic compounds, and in the protection of metals against corrosion-induced disintegration.

The study of the metal–electrolyte corrosion system taking into account the influence of the metal defects at different structural levels (from point defects to bulk-phase defects) shows that a quantitative estimate of the effect of the dissolution proper should also be performed at different levels. If a point defect or a single dislocation induce a local distortion of the lattice which undergoes a rapid and sharp attenuation in the vicinity of the defect, then this promotes the intensification of a local form of corrosion — an etch pit is formed (in the case of a grain boundary an etch groove is produced, whilst slit corrosion may develop at the DP–matrix interface). Elastic deformations arising from the boundaries of grains and inclusions embrace the entire bulk of the grain and the groups nearest to it. In the latter case, the study of the influence of defects on corrosion becomes possible in terms of the continuous approximation using the theory of elasticity.

It is apparently to be expected that studies of controllable chemical reactions on the thoroughly tested surfaces of bi- and tricrystals will be undertaken. This will lead to new possibilities for the specific synthesis of new chemical products.

This review has been written with the financial support of the 'Universities of Russia. Chemistry' (project 51) program.

References

1. W A T Clark, C J McMahon, R H Wagoner, R P Wei *Mater. Sci. Eng.* **83** 205 (1986)
2. R H Jones, in *4th International Conference on Hydrogen Effects on Material Behavior (Program and Abstracts)*, Jackson Lake, WY, 1989, p. 14
3. O N Markova, N D Tomashov, G P Chernova *Zashchita Met.* **29** 409 (1993)
4. G V Khaldeev *Ingibirovanie Rastvoreniya Metallov* (Inhibition of the Dissolution of Metals) (Moscow: Nauka, 1993)
5. H Gleiter, in *Atom Fracture. Proceedings of the NATO Advanced Research Institute, Caltoglio, 1983* p. 433
6. R W Baluffi, P D Bristowe *J. Phys.* **46** 267 (1985)
7. G A Chadwick, D A Smith (Eds) *Grain Boundary Structure and Properties* (New York: Academic Press, 1976)
8. A N Orlov, V N Pereverznev, V V Rybin *Granitsy Zeren v Metallakh* (Grain Boundaries in Metals) (Moscow: Metallurgiya, 1980)
9. B S Bokshtein, Ch V Kopetskii, L S Shvindlerman *Termodinamika i Kinetika Granits Zeren v Metallakh* (Thermodynamics and Kinetics of Grain Boundaries in Metals) (Moscow: Metallurgiya, 1986)
10. B S Bokshtein, Ch V Kopetskii, L S Shvindlerman, A N Orlov, L M Klinger, D A Gorbunov, V M Ivlev, Yu M Mishin, I M Azumovskii, S Z Bokshtein, A N Aleshin, S I Prokof'ev, B B Straumal, V E Fradkov *Struktura i Svoistva Vnutrennikh Poverkhnostei Razdela v Metallakh* (Structure and Properties of Internal Interfaces in Metals) (Moscow: Nauka, 1988)
11. A P Sutton *Int. Met. Rev.* **29** 377 (1984)

12. K Sangval *Travlenie Kristallov. Teoriya i Eksperiment* (Etching of Crystals. Theory, Experiment and Application) (Translated into Russian; Moscow: Mir, 1990)
13. L Beaunier, M Froment, C Vignaud *Electrochim. Acta* **25** 1239 (1980)
14. L Beaunier, M Froment, C Vignaud *J. Electroanal. Chem.* **119** 125 (1981)
15. R A Marcus *Annu. Rev. Phys. Chem.* **15** 155 (1964)
16. J Hirth, J Lothe *Theory of Dislocation* (Translated into Russian; Moscow: Atomizdat, 1972)
17. L V Spivak, N E Skryabina, M Ya Kats *Vodorod i Mekhanicheskoe Posledeistvie v Metallakh i Splavakh* (Hydrogen and Mechanical Secondary Action in Metals and Alloys) (Perm: Izd. Permsk. Univ., 1993)
18. M McLean, E K Hondros, in *Surface Mobilities of Solid Materials: Fundamental Concepts and Applications. Proceedings of the NATO Advanced Study Institute* (New York; Les Arcs, 1983) p. 459
19. R Dodd, J Eilbek, J Gibbon, H Morris *Soliton and Nonlinear Wave Equations* (Translated into Russian; Moscow: Mir, 1988)
20. B I Smirnov *Dislokatsionnaya Struktura i Uprochnenie Kristallov* (Dislocation Structure and Strengthening of Crystals) (Leningrad: Nauka, 1981)
21. K A Chishko *Fiz. Tverd. Tela* **23** 3028 (1981)
22. G V Khaldeev, L A Timofeeva, V V Kuznetsov *Poverkhnost'* **3** (3) 119 (1984)
23. V B Fedoseev *Poverkhnost'* **8** (17) 114 (1990)
24. G V Khaldeev, A B Volyntsev *Izv. Akad. Nauk SSSR, Met.* (3) 134 (1984)
25. A B Volyntsev *Nasledovannaya Mekhanika Dislokatsionnykh Ansamblei. Komp'yuternye Modeli i Eksperiment* (Inherited Mechanics of Dislocation Ensembles. Computer Models and Experiment) (Perm: Izd. Permsk. Univ., 1990)
26. J I Dickson, S Turenne, H Bande, G L Esperance *Mater. Sci. Eng.* **89** L31 (1987)
27. A V Pevneva, G V Khaldeev, V V Kuznetsov *Zashchita Met.* **12** 50 (1976)
28. D M Drazic *Mod. Aspects Electrochem.* **19** 69 (1989)
29. T Ohnori *Denki Kagakuyobi Fogyo Butsure Kagaku* **56** (3) 181 (1988)
30. L-B Le, O Bittori *J. Chem.* **66** 1525 (1988)
31. G V Khaldeev, S M Reshetnikov, V F Knyazeva, V V Kuznetsov *Zh. Prikl. Khim.* **53** 1298 (1980)
32. I K Marshakov, A F Vvedenskii, V Yu Kondrashin, G A Bokov *Anodnoe Rastvorenie i Selektivnaya Korroziya Splavov* (Anodic Dissolution and Selective Corrosion of Alloys) (Voronezh: Izd. Voronezh. Gos. Univ., 1988)
33. A N Kuzyukov *Zashchita Met.* **30** 166 (1994)
34. K Vetter *Electrochemische Kinetic* (Translated into Russian; Moscow: Khimiya, 1967)
35. V I Arnol'd *Teoriya Katastrof* (Catastrophe Theory) (Moscow: Nauka, 1990)
36. P J Ortoleva *J. Electrochem. Soc.* **130** 621 (1983)
37. O Peschke, M U Kleinke, F Galembeck, M A Tenan *Langmuir* **6** 829 (1990)
38. M N Polukarov *Zh. Prikl. Khim.* **21** 611 (1948)
39. G V Khaldeev, V V Kamelin *Dokl. Akad. Nauk SSSR* **310** 653 (1990)
40. G V Khaldeev, V V Kamelin *Usp. Khim.* **61** 1623 (1992) [*Russ. Chem. Rev.* **61** 889 (1992)]
41. Y Wang, S L Hudson, N I Jaeger *J. Electrochem. Soc.* **137** 485 (1990)
42. A J Perlstein, J A Johnson *J. Electrochem. Soc.* **136** 1290 (1989)
43. A D Konyukhov, V E Konyukhov *Zashchita Met.* **30** 212 (1994)
44. J Marsden, M McKraken *Bifurcation of Birth-Cycle and Its Application* (Translated into Russian; Moscow: Mir, 1980)
45. W W Mullins *J. Appl. Phys.* **28** 333 (1957)
46. V V Pokropivnyi, V V Skorokhod *Dokl. Akad. Nauk Ukrain. SSR, Ser. A* (12) 68 (1987)
47. W W Mullins *Trans. Metall. Soc. AIME* **218** 354 (1960)
48. L Ratke, H J Fogel, in *Proceedings of the VII European Symposium on Materials and Fluid Science, London, 1989* p. 497
49. H L Huang, J S Yang *J. Vac. Sci. Technol.* **A5** 1487 (1987)
50. Z B Pfeil *Proc. Roy. Soc., Math. Phys. Sci., A* **112** 182 (1926)
51. T Mimaki, Y Narazawa, S Hashimoto, S Miura *Met. Abstr. Light Met. Alloys* **24** 72 (1991)
52. M Yamashita, T Mimaki, S Hashimoto, S Miura *Met. Abstr. Light Met. Alloys* **24** 69 (1991)
53. M Yamashita, M Yoshioka, T Mimaki, S Hashimoto, S Miura *Met. Abstr. Light Met. Alloys* **24** 75 (1991)
54. H Vehoff, H Stenzel, P Neumann *Z. Metallkunde* **78** 550 (1987)
55. D Wolf *Physica B* **131** 53 (1985)
56. Th Karakostas, G L Bleris, J G Antonopoulos *Phys. Techn. Semicond.* **73** 26 (1979)
57. V M Knyazheva, in *Novye Dostizheniya v Oblasti Teorii i Praktiki Protivokorrozionnoi Zashchity Metallov* (Recent Advances in the Theory and Practice of Anticorrosion Protection of Metals) (Moscow: Nauka, 1981) p. 49
58. P Merino, X R Novoa, G Pena, E Porto, L Espada *Mater. Sci. Technol.* **9** 168 (1993)
59. V M Mil'man, Candidate Thesis in Chemical Sciences, Physicochemical Institute, Moscow, 1991
60. G S Was *Corrosion (USA)* **46** 319 (1990)
61. E T Shapovalova, M Yu Ustimenko *Zashchita Met.* **29** 231 (1993)
62. V Kain, in *Workshop on Failure Analysis, Corrosion Production, and Metallography, Bombay, 1992: FACORMET-92* p. 107
63. T -J Chuang, K I Kagawa, J R Rice, L B Sills *Acta Metall.* **27** 265 (1979)
64. G Sundararajan, P G Shewmon *Met. Trans. A, Phys. Metall. Mater. Sci.* **12** 1761 (1981)
65. A M Klinger *Poverkhnost'* **2** (4) 17 (1983)
66. Ph Joel *J. Electrochem. Soc.* **139** 51 (1992)
67. B Landa, H K Birubaum *Acta Metall.* **35** 2537 (1987)
68. A B Shein, G V Khaldeyev, in the *4th International Conference on Hydrogen Effects on Material Behavior (Program and Abstracts)*, Jackson Lake, WY, 1989, p. 18
69. G C Pain, F W Averill *Phys. Rev. Lett.* **58** 234 (1987)
70. M Hashimoto, Y Ishida, R Yamamoto, M Doyama, T Fujiwara *Scr. Metall.* **16** 267 (1982)
71. H J Grabke, in *Chemical and Physical Fractures: Proceedings of the NATO Advanced Research Workshop, Bad Reichenhall, 1987* p. 388
72. K Yamanaka *Corros. Eng.* **41** 461 (1992)
73. I Olefjord, C R Clayton *ISIJ Int.* **31** 134 (1991)
74. R F A Jargelins-Petterson, in the *12th Scandinavian Corrosion Congress and EUROCORR'92, Espoo, 1992* p. 119
75. W Schwenk *Stahl Eisen* **111** 114 (1991)
76. U Erb, H Gleiter, G Schurtzgebet *Acta Metall.* **30** 1377 (1982)
77. R Maurer, U Erb, H Gleiter *Mater. Sci. Eng.* **63** L13 (1984)
78. B W Bennett, H W Pickering *Met. Trans. A, Phys. Metall. Mater. Sci.* **18** 1117 (1987)
79. G V Khaldeev, V F Knyazeva, A B Volyntsev, L V Spivak *Zashchita Met.* **15** 717 (1979)
80. A V Galina, V E Fradkov, L S Shvindlerman *Poverkhnost'* **6** (1) 100 (1988)
81. V V Kuznetsov, G V Khaldeev, V I Kichigin *Navodorozhivanie Metallov v Elektrolitakh* (Saturation of Metals with Hydrogen in Electrolytes) (Moscow: Mashinostroenie, 1993)
82. L T Berezhnitskii, N G Stashchuk *Fiz-Khim. Mekh. Mater.* **18** 61 (1982)
83. A I Kitaigorodskii *Smeshannye Kristally* (Mixed Crystals) (Moscow: Nauka, 1983)
84. G Leibfried, N Broier *Point Defects in Metals* (Translated into Russian; Moscow: Mir, 1981)
85. I M Lifshits, V V Slezov *Zh. Eksp. Teor. Fiz.* **35** 479 (1958)
86. S Redner, D Ben-Avraham, B Kahng *J. Phys. A, Math. Gen.* **20** 1231 (1987)